Journal of Geochemical Exploration 270 (2025) 107641

Contents lists available at ScienceDirect

Journal of Geochemical Exploration

journal homepage: www.elsevier.com/locate/gexplo

The source of lithium in connate fluids: Evidence from the geothermal reservoir at Soultz-sous-Forêts, Upper Rhine Graben, France

Michèle Jungmann [a,b,*], Benjamin F. Walter [a,b,c], Elisabeth Eiche [a,b], R. Johannes Giebel [d,e], Jochen Kolb [a,b]

[a] Geochemistry and Economic Geology, Institute of Applied Geosciences, Karlsruhe Institute of Technology, Karlsruhe, Germany
[b] Laboratory for Environmental and Raw Materials Analysis, Institute of Applied Geosciences, Karlsruhe Institute of Technology, Karlsruhe, Germany
[c] Eberhard Karls University Tübingen, Petrology and Mineral Resources, Schnarrenbergstraße 94-96, 72074 Tübingen, Germany
[d] Technische Universität Berlin (TUB), Institute of Applied Geosciences, Ernst Reuter Platz 1, 10587 Berlin, Germany
[e] University of the Free State, Department of Geology, 250 Nelson-Mandela-Drive, Bloemfontein 9300, South Africa

ARTICLE INFO

Keywords:
Fluid-rock interaction
Geothermal system
Lithium
Brine
Connate fluid
Mineral system

ABSTRACT

Geothermal brines in the Upper Rhine Graben have been used as a spa or for salt production since Roman times. Heat and power are generated in geothermal power plants since 2007. Recently, their elevated Li-content has additionally attracted economic interest. This increased interest is in contrast with our understanding of the geological-hydrothermal evolution. We use petrology, major and trace element mineral chemistry and mass balance calculation from drill cores that intersect granitic geothermal reservoir rocks at Soultz-sous-Forêts between Strasbourg and Karlsruhe to shed light on fluid-rock interaction in a reservoir that is actively used for heat and power generation. The alkali feldspar and the two-mica granite in the reservoir have a typical plagioclase, K-feldspar, quartz, biotite and muscovite assemblage with some accessories of titanite, apatite and zircon. Two hydrothermal alteration events are distinguished: (1) albitization of the feldspars; (2) distal replacement of feldspars by sericite and calcite, of biotite by chlorite and titanite; and proximal to hydrothermal veins replacement of the feldspars by sericite and kaolinite. Event 2 feldspar alteration quantitatively releases Pb and Ba to the fluid, whereas Rb, Cs, Sr and Zn show different behaviour depending on whole-rock and mineral composition. Event 2 biotite-chlorite alteration releases Li, Rb, Cs, Sr, Ba, Zn and Pb to the fluid. Mass balance calculation indicates that Si, Fe, Ca, K, Rb, Sr, Zn and Pb contents of the Soultz-sous-Forêts geothermal brine may be explained by fluid-rock interaction in the reservoir. However, the reservoir rock volume that needs to be leached in order to reach recent brine composition varies by several orders of magnitude between the different elements. Many of the elements may be leached during hydrothermal alteration, however in particular Li and Cs require unrealistic fluid-rock ratios of >1/300. These considerations indicate that Na, Ca, Li, Cs and Ba need an additional external source. Based on this, we propose a model where Middle Triassic bittern brines already enriched in Li, Rb, and Cs reacted with the reservoir rocks during hydrothermal event 2 and subsequently mixed with Jurassic-Cretaceous marine water that dissolved evaporites during downward migration. This agrees with Jurassic-Cretaceous illite ages from various sites in the Black Forest and indicates a complex ~150 m.y. hydrothermal evolution for the brines. There is likely no single source of Li, and it is likely derived from complex fluid-rock interaction with the sedimentary (evaporite) and, less importantly, the crystalline strata of the Upper Rhine Graben. Critical for Li-resource development is the complex hydrothermal history of connate fluids that interacted with sedimentary strata and the preservation in deep-seated reservoirs.

1. Introduction

The Upper Rhine valley stretches from Basel at the Swiss-German border in the south along the French-German border to Frankfurt in the north for >300 km (Fig. 1). It is situated in the Upper Rhine Graben which is part of the European Cenozoic Rift System that extends from the Rhône River estuary to the North Sea (Fig. 1). The Upper Rhine Graben is bound to the south by a transform fault that connects it to the Bresse

* Corresponding author at: Geochemistry and Economic Geology, Institute of Applied Geosciences, Karlsruhe Institute of Technology, Karlsruhe, Germany.
E-mail address: michele.jungmann@kit.edu (M. Jungmann).

https://doi.org/10.1016/j.gexplo.2024.107641
Received 3 June 2024; Received in revised form 9 November 2024; Accepted 20 November 2024
Available online 27 November 2024

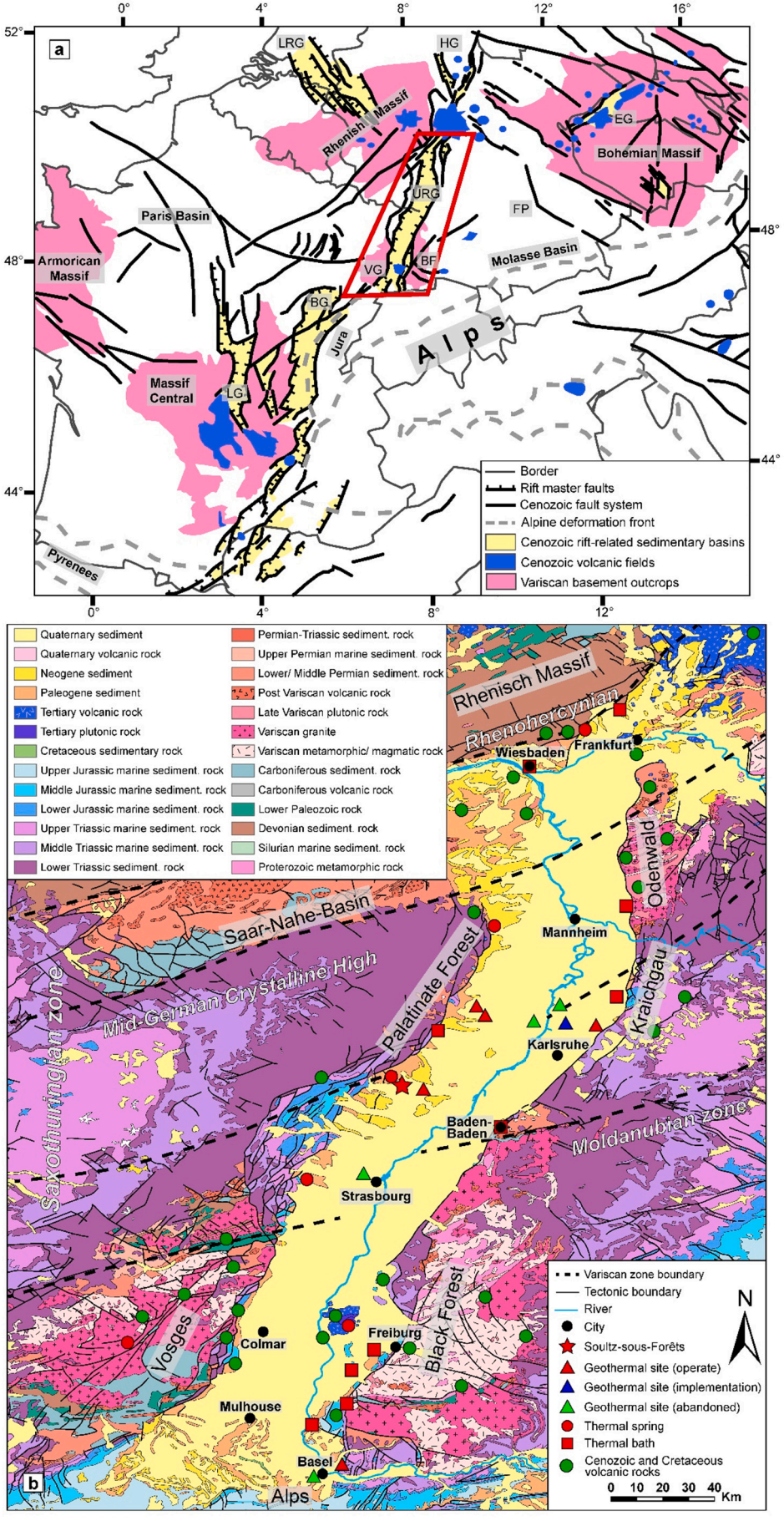

(caption on next page)

Fig. 1. a) European Cenozoic Rift System (ECRIS) with the Upper Rhine Graben (adapted from Ziegler and Dèzes, 2005 and Timar-Geng et al., 2006). BF Black Forest, BG Bresse Graben, EG Eger Graben, FP Franconian Platform, HG Hessian Grabens, LG Limagne Graben, LRG Lower Rhine Graben, OW Odenwald, URG Upper Rhine Graben, VG Vosges. b) Geological map of the Upper Rhine Graben with the rift valley and the Variscan orogen forming the rift shoulders (adapted from Voges et al., 2006). Cenozoic and Cretaceous volcanic rocks after Binder et al. (2022).

Graben, it transects the Variscan Orogen and is bound to the north by a triple junction marked by the Vogelsberg volcano north-east of Frankfurt (Fig. 1; Geyer et al., 2011; Voges et al., 2006; Ziegler, 1992; Ziegler et al., 2004). It is filled by a maximum column of 6500 m Permo-Triassic to Holocene sedimentary rocks and sediments (Fig. 1; Geyer et al., 2011; Voges et al., 2006).

Several spas like Wiesbaden or Baden-Baden are located at the margin of the Upper Rhine Graben (Fig. 1). Numerous Roman remnants indicate that the warm springs have been intensely used at least since that time (Becker and Reischmann, 2021; Geyer et al., 2011; He et al., 1999). Moreover, saline brines have been used to produce salt at several locations (e.g. Bruchsal; Bad Nauheim; Becker and Reischmann, 2021; Geyer et al., 2011). The first commercial geothermal power plant in the Upper Rhine Graben opened in Landau in 2007 (Agemar et al., 2014; Stober and Bucher, 2015a). The Triassic sandstones and the Variscan crystalline rocks have the highest potential for geothermal energy production (Agemar et al., 2014; Sanjuan et al., 2016, 2022). Largest thermal anomalies are located in the area of Soultz-sous-Forêts and Landau (Agemar et al., 2013; Baillieux et al., 2013; Stober and Bucher, 2015a). At Soultz-sous-Forêts, a thermal gradient of 120 °C/km in the sedimentary rocks and 30 °C/km in the granite leads to approximately 200 °C at 5000 m depth (Fig. 2; Agemar et al., 2012, 2013; Baillieux et al., 2013; Genter et al., 2003). The political decision in Germany to shift to renewable energy production resulted in an increased interest in geothermal energy production since it provides electric power constantly (base load) and heat independently from the weather (BMWK, 2022; Fridleifsson, 2001; Held et al., 2014). These advantages result in an increased number of exploration campaigns in the Upper Rhine Graben and the development of various new projects (e.g.; Graben Neudorf, Fig. 1; Bundesverband Geothermie e.V., 2023).

The brines that are used in the geothermal power plants were recently recognized as considerable lithium (Li) resource with 160–210 mg/L Li (e.g. Reich et al., 2022; Sanjuan et al., 2016, 2022; Steiger et al., 2022), which further intensified exploration activities. Vulcan Energy Resources claims that they have 26.6 Mt. Lithium Carbonate Equivalent (LCE) as resources in their Phase One license areas (LGB-RLP, 2013; Vulcan Energie Ressourcen GmbH, 2023). In the EnBW power plant Bruchsal it is estimated that 1000 t LCE can be produced at industrial scale annually (UnLimited project, 2022).

Modern economic geology research applies the mineral systems approach to explain the formation of ore deposits in a holistic way (McCuaig et al., 2010; McCuaig and Hronsky, 2014). This importantly addresses the source of metals and fluids in hydrothermal systems. The geothermal fluids in the Upper Rhine Graben are an expression of an active hydrothermal system (Loges et al., 2012). The difference to rock-hosted Li ore deposits is that Li is still in solution and does not form Li-rich minerals. A reliable resource estimation of dissolved Li in the brines requires a thorough understanding of its origin and temporal evolution.

International projects analysed fluids in sedimentary basins, particularly in Europe and North America (Coffey et al., 2021; Dugamin et al., 2023; Fontes and Matray, 1993). Their findings resulted in general theories about Li origin and the temporal evolution of fluids in sedimentary basins: (1) Li-enrichment in the fluid due to diagenetic fluid-rock interaction, including water uptake and Li release from host minerals; (2) high Li-contents in the fluid source, paleo-seawaters may have had higher compositions than today's seawater (Weldeghebriel and Lowenstein, 2023); (3) Li-enrichment through evaporation (seawater/salt lakes). In a global analysis of sedimentary basin fluids, Dugamin et al. (2023) identify four different fluid end members: (1) low-salinity waters (meteoric waters, recharge waters), (2) seawater, (3) evaporated seawater and (4) high-salinity waters (reaching halite saturation) with high Li contents. Comparing sedimentary basin formation waters and salt lakes, it is found that the high Li-content in the salt lake brines can only be achieved if primary evaporitic brines interacted with leachable Li in rocks or minerals (volcanic rocks, Li-rich clay beds or detrital, Li-rich phyllosilicates dispersed in siliciclastic rocks) and are not diluted subsequently (Coffey et al., 2021; Dugamin et al., 2023; Macpherson, 2015; Marza et al., 2024; Munk et al., 2016; Phan et al.,

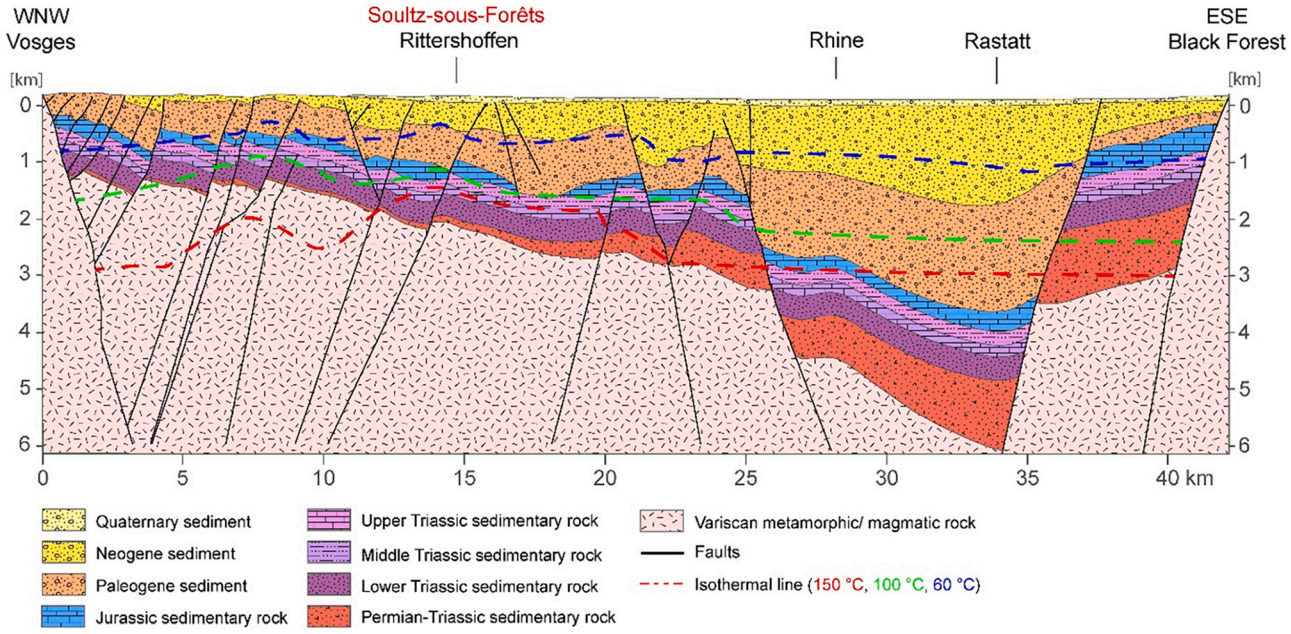

Fig. 2. WNW-ESE cross-section through the rift centre along Rastatt and Soultz-sous-Forêts (adapted from Anders et al., 2013b). The cross-section illustrates isotherms and the rift structure cross-cutting stratigraphy (adapted from Anders et al., 2013b).

2016). Less enriched Li brines consist of a saline component (seawater or evaporated seawater (primary brine)) that is diluted by low-salinity water (Dugamin et al., 2023; Fontes and Matray, 1993). These fluids can further be enriched in Li through water-rock interactions. Accordingly, Sanjuan et al. (2022) and Dugamin et al. (2024) conclude that fluid-assisted decomposition of mica and clay minerals leads to Li-enrichment in the fluids of the European sedimentary basins and the Upper Rhine Graben.

The geochemical provenance and the evolution of the Li-bearing brine can be studied best at Soultz-sous-Forêts because drill cores from reservoir rocks and brine are available for detailed petrography and geochemical investigation. Therefore, the reservoir of Soultz-sous-Forêts is used as a natural laboratory in this study.

Contradicting models for the evolution of the hydrothermal system in the Upper Rhine Graben have been developed. Hydrothermal leaching experiments indicate that at least some of the Li in the geothermal brines is released by hydrothermal alteration of the granitic reservoir rocks (Drüppel et al., 2020; Schmidt et al., 2018). However, lithium isotopes indicate a Li-source in carbonated sedimentary rocks of the Buntsandstein and Sr- and Nd- isotope data indicate fluid-rock interaction with the sandstones (Sanjuan et al., 2010, 2016, 2022). Lithium is likely sourced from biotite dissolution in the Buntsandstein sandstone (Sanjuan et al., 2016, 2022), which locally contains close to 80 mg/kg lithium (Kölbel et al., 2023). The fluid is considered to represent a Mesozoic or Cenozoic brine that is derived from seawater evaporation up to halite saturation mixed with meteoric water, including probable halite dissolution or mixing with brine that dissolved halite (Dugamin et al., 2023; Pauwels et al., 1993; Sanjuan et al., 2016). In addition, mixing with a deep brine that derived from fluid-rock interaction with the Variscan crystalline rocks is considered (Stober and Bucher, 1999a, b, 2015a). The models of the fluid pathways are in particular contradictory: (1) The fluid migrated downwards and chemically equilibrated with the lower Triassic Buntsandstein sandstone at 225 ± 25 °C in the rift centre, where this unit is deepest (Dugamin et al., 2024; Pauwels et al., 1993; Sanjuan et al., 2010, 2016). From there, the fluid migrated through a complex, but still poorly defined system of deep faults to the Variscan granite at the northwestern graben margins (Pauwels et al., 1993; Sanjuan et al., 2010, 2016). (2) The fluid originates from the rift shoulders and migrates topographically induced downwards to the rift centre. From there, it migrated along faults and fractures into the reservoirs in upwelling zones, which is indicated by natural thermal springs at the surface (Stober and Bucher, 2015a, 2015b).

This controversy shows that origin, pathway and geochemical evolution of the fluid are still unresolved. Therefore, this contribution aims to fill existing knowledge gaps on the alteration interface between the geothermal brines and their reservoir rocks.

Petrographical, geochemical and mineral chemistry data have been gathered from drill core samples of the geothermal reservoir rocks at Soultz-sous-Forêts to evaluate the hypothesis that Li originates from fluid-rock interaction in the geothermal reservoir. The combination of the applied analytical methods and mass balance calculations allows to build a new holistic model for complex fluid-rock interaction between granite and connate fluid. In order to determine whether Li and other trace elements are enriched in the fluid or incorporated in the hydrothermal alteration minerals, the initial mineral composition will be directly compared with the trace element contents in the alteration minerals. We show that Li, Cs and Na need a major source outside the reservoir rocks of Soultz-sous-Forêts, whereas Si, K, Rb, Sr, Ba, Zn and Pb may be sourced in these rocks depending on whole rock and mineral composition.

2. Regional geology

The Upper Rhine Graben in the European Cenozoic Rift System represents a rift, which is between 30 and 50 km wide and up to 6500 m deep (surface to top Variscan crystalline rocks) (Figs. 1, 2; Anders et al., 2013a; Geyer et al., 2011; LGRB-Kartenviewer, 2021). The rift shoulders are characterised by crystalline rocks of the Variscan Orogen and Mesozoic sedimentary rocks (Fig. 1). In the south, the rift is bound by the Swiss Alps (Fig. 1).

2.1. Geology of the Upper Rhine Graben

The basement of the rift is characterised by crystalline rocks of the Variscan Orogen as indicated by numerous drill intersects and seismic data (Agemar et al., 2014; Anders et al., 2013a; Boy and Steingötter, 2005; Geyer et al., 2011; Sanjuan et al., 2016; Stober and Bucher, 1999a, 2007). From south to north, the Upper Rhine Graben transects the Moldanubian, Saxothuringian, Mid-German Crystalline High and Rhenohercynian zones of the Variscan Orogen (Fig. 1; Geyer et al., 2011; Skrzypek et al., 2014; Voges et al., 2006; Ziegler et al., 2004).

In the Moldanubian zone, intermediate to high-grade metamorphic paragneiss, eclogite, amphibolite, orthogneiss and late-Variscan granite dominate (Altherr et al., 2000; Geyer et al., 2011; Hann et al., 2003; Lardeaux et al., 2014; Skrzypek et al., 2014). As part of the Moldanubian zone, the Badenweiler-Lenzkirch zone and parts of the southern Vosges are dominated by low-grade metamorphic granite and metasedimentary rocks (Geyer et al., 2011; Lardeaux et al., 2014; Skrzypek et al., 2014; Vaida et al., 2004). The reservoir rocks at Soultz-sous-Forêts belong to the Moldanubian zone and are represented by 331 ± 9 Ma granite (U-Pb zircon data; Alexandrov et al., 2001). The Saxothuringian zone consists of phyllite and mica schist (Geyer et al., 2011; Skrzypek et al., 2014). The Mid-German Crystalline High (Saxothuringian) comprises high-grade metamorphic paragneiss and mica schist, low-grade meta-conglomerate, meta-breccia and late-Variscan granite (Becker and Reischmann, 2021; Boy and Steingötter, 2005; Geyer et al., 2011; Skrzypek et al., 2014; Tabaud et al., 2014, 2015). The northern Upper Rhine Graben is bound by the Rhenish Massif of the Rhenohercynian zone, which is dominated by metapelite, meta-greywacke and quartzite (Becker and Reischmann, 2021).

These rocks are locally covered by Permo-Carboniferous but generally by Triassic rocks. The Permo-Carboniferous sedimentary rocks comprise thin beds of coal and arkose, conglomerate, sedimentary breccia, and sandstone (Aretz et al., 2016; Geyer et al., 2011). During the Lower Permian (Rotliegend), red sandstones formed in distinct intramountainous depressions and graben structures (Kraichgau, Schramberg, and Saar-Nahe, Figs. 1, 2) with a local thickness of up to 1000 m (Anders et al., 2013a; Becker and Reischmann, 2021; Geyer et al., 2011; Rupf and Nitsch, 2008). The sandstone is locally overlain by pyroclastic rocks and lava flows of basaltic and rhyolitic composition (300–286 Ma Rb-Sr and Ar-Ar (mica), Becker and Reischmann, 2021; Boy and Steingötter, 2005; Geyer et al., 2011; Lippolt et al., 1983; Lützner et al., 2012; Nitsch and Zedler, 2009; Ziegler et al., 2004). In the northern Upper Rhine Graben, the Upper Permian (Zechstein, thickness 0–200 m) is characterised by evaporite and claystone (Becker and Reischmann, 2021). To the south, terrestrial sedimentary rocks of conglomerate, arkose, sandstone and claystone dominate (Geyer et al., 2011; Nitsch and Zedler, 2009). They are overlain by Lower Triassic sandstone (Buntsandstein, thickness 50–500 m), which is covered by alternating units of limestone, marl, evaporite (gypsum, anhydrite and halite) and claystone of the Middle Triassic (Muschelkalk, thickness 160–200 m). These rocks are, in turn, overlain by sandstone, claystone and dolomite-bearing marl of the Upper Triassic (Keuper, thickness 130–300 m). The Jurassic (thickness 300–700 m) is mainly characterised by claystone and marine limestone. Continuous sedimentation ended in the Cretaceous when the area was affected by uplift (Figs. 1, 2; Anders et al., 2013b; Becker and Reischmann, 2021; Boy and Steingötter, 2005; Geyer et al., 2011; Rupf and Nitsch, 2008). As a consequence of Cenozoic rifting, the Upper Rhine Graben became a depocenter again and a 100–4000 m thick Cenozoic sedimentary package including mainly marine (e.g. evaporite reaching the bitter salt stage in the Pechelbronn formation) and continental clastic sedimentary rocks was formed (Figs. 1, 2; Anders

et al., 2013b; Geyer et al., 2011; Rupf and Nitsch, 2008). Cretaceous and Cenozoic igneous rocks of the Central European Volcanic Province occur in numerous diatremes and volcanos along the rift shoulders and within the rift (Becker and Reischmann, 2021; Binder et al., 2022; Geyer et al., 2011; Giebel et al., 2019). The youngest Quaternary clastic sedimentary rocks are of fluviatile, lacustrine and aeolian origin (thickness 0–500 m; Becker and Reischmann, 2021; Geyer et al., 2011).

Five hydrothermal mineralization events are distinguished in the Black Forest (Baatartsogt et al., 2007; Pfaff et al., 2010; Scharrer et al., 2021; Walter et al., 2015, 2016, 2017, 2018a, 2018b, 2019, 2020a, 2020b): (1) Carboniferous quartz-tourmaline veins; (2) Permian quartz veins; (3) Triassic-Early Jurassic quartz-hematite veins; (4) Middle Jurassic-Cretaceous fluorite-quartz-baryte and baryte-quartz veins; and (5) Cenozoic quartz-baryte-fluorite veins and the Wiesloch Mississippi-Valley-type (MVT) deposit.

The Carboniferous quartz-tourmaline veins are related to granite of similar age and to contemporaneous propylitic alteration (Marks et al., 2013; Glaas et al., 2019; Vidal et al., 2018). Argillic alteration in fracture and fault zones of the Variscan crystalline rocks is related to the hydrothermal 2–5 events (Bartier et al., 2008; Ledésert et al., 2010; Schleicher et al., 2006). Illite is dated at 196–142 Ma (Ar-Ar, K-Ar; Bossennec et al., 2021a, 2021b; Brockamp et al., 2003, 2011; Brockamp and Clauer, 2005; Meyer et al., 2000; Walter et al., 2016, 2019).

The hydrothermal paleo-fluids trapped in Jurassic-Cretaceous veins of the Black Forest show a binary mixture of two fluids originally representing seawater, subsequently modified by fluid-rock interaction (dissolution of Triassic evaporites, mineral precipitation or albitization) (Scharrer et al., 2021). This resulted in two components of bittern, halite dissolution brines with different salinities, in which elements are dissolved at various concentrations (Bons et al., 2014; Epp et al., 2019; Scharrer et al., 2021; Walter et al., 2016, 2017, 2018a, 2019). Fluid-inclusion data of the Cenozoic hydrothermal veins show that the fluids represent a complex mixture of chemically modified fluids from various aquifers (Scharrer et al., 2021; Walter et al., 2016, 2017, 2018a, 2019). Nine different stratigraphic units are exploitable as geothermal reservoirs (Anders et al., 2013a; Frey et al., 2022; Geyer et al., 2011; Loges et al., 2012; Sanjuan et al., 2016; Stober and Bucher, 2015a): (1) the Variscan crystalline basement; (2) Permo-Carboniferous sandstone; (3) Triassic sandstone (Buntsandstein) and (4) limestone (Muschelkalk); (5) Upper and (6) Middle Jurassic limestone, and three Cenozoic units namely (7) Niederrödern Formation; (8) Froidefontain Formation and (9) Pechelbronn Formation. Currently, brines derived from the Variscan crystalline basement, Permo-Carboniferous sandstone and Triassic sandstone are used in geothermal power plants (Anders et al., 2013a; Aquilina et al., 1997; Sanjuan et al., 2016). The other six geothermal reservoirs are used either as sources for warm springs or wells of thermal spas (Göb et al., 2013; He et al., 1999; Loges et al., 2012). Dissolved Li resources are located in the Variscan crystalline basement and Triassic sandstones with 41–210 mg/L Li (Aquilina et al., 1997; Pauwels et al., 1993; Sanjuan et al., 2016, 2022).

2.2. Soultz-sous-Forêts: geothermal power plant and geology

Soultz-sous-Forêts is located on the western side of the Upper Rhine valley between Karlsruhe and Strasbourg (Fig. 1). Geophysical exploration defined a thermal anomaly, which was the target of drilling campaigns from 1987 to 2004 (Agemar et al., 2013; Baillieux et al., 2013; Dezayes et al., 2005b; Gérard et al., 2006). Five boreholes were drilled (Fig. 3; EPS-1, GPK-1 to 4). The latter three reach a depth of approx. 5000 m and are used for power production today (Gérard et al., 2006; MEET project, 2022; Sanjuan et al., 2010). In 2008, a research power plant was commissioned, which was replaced by a commercial power plant in 2016 (Dezayes et al., 2005b; Genter et al., 2010; Held et al., 2014; Hooijkaas et al., 2006; MEET project, 2022). The 200 °C hot fluid is extracted via an open borehole section in GPK-2 from bottom hole to approximately 4500 m at the contact of two-mica granite and

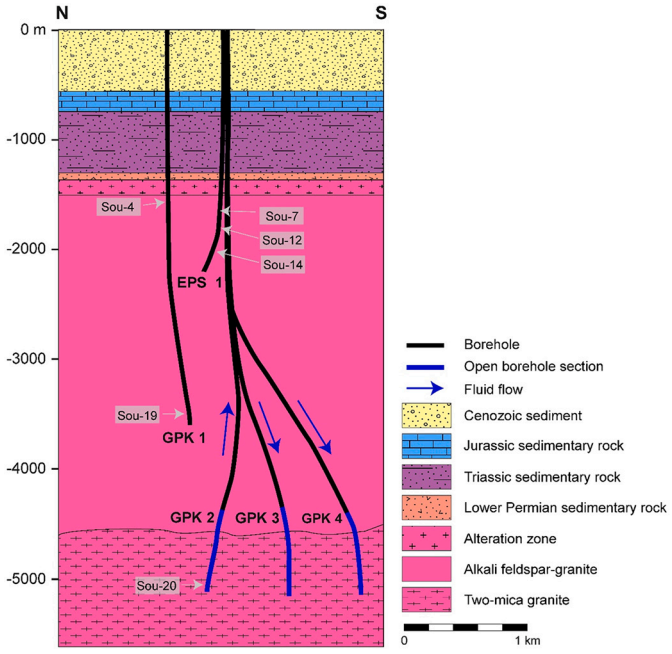

Fig. 3. Schematic cross-section at the Soultz-sous-Forêts geothermal power plant. The five wells including production (GPK-2) and injection wells (GPK-3, GPK-4) with open borehole sections and the sample locations are shown. After Dezayes et al. (2005a), Held et al. (2014) and Ledésert and Hébert (2020).

alkali feldspar-granite (Fig. 3; Ledésert and Hébert, 2020; Sanjuan et al., 2010). To increase productivity, this petrothermal system (Jolie et al., 2021; Moeck, 2014) was chemically and hydraulically stimulated (Genter et al., 2010; Sanjuan et al., 2010; Schill et al., 2017; Vidal and Genter, 2018).

The two-mica granite is composed of fine-grained quartz, K-feldspar, plagioclase, biotite, muscovite and accessory minerals (Dezayes et al., 2005a; Dugamin et al., 2024; Gardien et al., 2016; Genter et al., 1997; Genter et al., 1999). The contact with the alkali feldspar-granite at a depth of ~4700 m is intrusive (Dezayes et al., 2005a; Hooijkaas et al., 2006). This granite is composed of K-feldspar megacrysts in a coarse-grained, epigranular texture of quartz, plagioclase, K-feldspar, biotite, amphibole and accessory minerals (Dugamin et al., 2024; Gardien et al., 2016; Genter et al., 1997; Hooijkaas et al., 2006). Whole rock geochemical data indicate granite/granodiorite to monzogranite composition (Dugamin et al., 2024; Genter et al., 1997; Stussi et al., 2002).

The two-mica granite and the alkali feldspar-granite show two different types of hydrothermal alteration: (1) large-scale pervasive hydrothermal alteration; and (2) hydrothermal alteration along veins and fractures (vein alteration; Genter et al., 1997). The pervasive alteration is characterised by the replacement of feldspar by a complex intergrowth of illite and muscovite (in the following termed sericite), and biotite by chlorite (propylitic alteration after Dezayes et al., 2005a; Dugamin et al., 2024; Genter et al., 1999; Glaas et al., 2019). The vein alteration strongly modified the primary granite texture. Typical minerals are quartz, clay minerals (illite, smectite, tosudite), calcite, hematite, sulfide ± chlorite (Bartier et al., 2008; Dezayes et al., 2005a; Dugamin et al., 2024; Genter et al., 1997; Ledésert et al., 1999, 2010).

The top of the alkali feldspar-granite at ~1500 m depth is logged as an alteration zone and interpreted as Permian weathering (Fig. 3; Genter et al., 1997; Hooijkaas et al., 2006). It is characterised by iron hydroxides and hematitization of biotite, magnetite and amphibole (Genter et al., 1997; Hooijkaas et al., 2006). Variable illite Ar-Ar data indicate hydrothermal alteration at different stages during the late Triassic to Cretaceous (Clauer et al., 2008; Schleicher et al., 2006).

At ~1300–1400 m depth, the granite is unconformably overlain by

Permian to Cenozoic sedimentary rocks (Fig. 3; Aichholzer et al., 2016; Aichholzer et al., 2019; Genter et al., 1997). The Permian rocks consist of a ~70 m thick layer of dark red, clayey sandstone (Annweiler Formation; Aichholzer et al., 2016; Aichholzer et al., 2019; Anders et al., 2013a). This is overlain by 390 m thick aeolian and fluviatile red sandstone of the Lower Triassic (Buntsandstein). The Middle Triassic limestone and marl have a thickness of ~160 m, while the Upper Triassic red and green claystone reach a thickness of ~70 m. The marine Jurassic marl and massive limestone reach a thickness of ~175 m. The Cenozoic sedimentary rocks lie unconformably on the Jurassic rocks and consist mainly of clay- and sandstone with intercalations of evaporite. The youngest sediments consist of Quaternary sand and clay (Aichholzer et al., 2016; Anders et al., 2013a).

2.3. Geochemistry of the Soultz-sous-Forêts geothermal fluid

The fluid used in the Soultz-sous-Forêts power plant is a Na-Cl brine with a salinity of 99 g/L TDS and a pH of 5 (at 37 °C; Sanjuan et al., 2016). The major elements besides Na (28.1 g/L) are K (3195 mg/L) and Ca (7225 mg/L). Iron (25.5 mg/L), Al (93.9 mg/L) and SiO_2 (201 mg/L) are minor elements. The alkaline and alkaline earth elements Li (173 mg/L), Rb (25.7 mg/L), Cs (14.9 mg/L) and Mg (131 mg/L), Sr (455 mg/L), Ba (5070 μg/L) as well as Mn (16.9 mg/L), Cu (1.44 μg/L), Zn (2168 μg/L) and Pb (137 μg/L) occur in traces or as minor constituents (Sanjuan et al., 2016). The fluid inclusion composition covers a wide range than the Soultz-sous-Forêts geothermal fluid and shows Li concentrations of up to 1000 ppm (Dugamin et al., 2024). The data indicate mixing trends between evaporated marine brines, which evolved by fluid-rock interaction in the granite, and dilute meteoric fluids.

The stable isotope data of the hydrothermal fluid yields $\delta D = 44.0$ ‰, $\delta^{18}O = -2.4$ ‰, $\delta^{34}S_{(SO4)} = 15.9$ ‰ and $\delta^{18}O_{(SO4)} = 5.1$ ‰ (Sanjuan et al., 2016). The data indicate mixing of Mesozoic and/or Cenozoic marine brines with meteoric fluid and subsequent halite dissolution as fluid source for Soultz-sous-Forêts (Sanjuan et al., 2016, 2022). The δ^7Li values are −0.4, −0.1, 0.6 and 1.4 ‰, which is different from typical marine signatures (Sanjuan et al., 2010, 2016, 2022). The data are explained by fractionation during fluid-rock interaction with carbonated sedimentary rocks and Li being derived from mica (Sanjuan et al., 2010, 2016, 2022). The $^{87}Sr/^{86}Sr$ ratio of the fluid is 0.711319, which is not radiogenic enough to be explained by fluid-rock interaction solely by the two-mica granite ($^{87}Sr/^{86}Sr = 0.717312$; Sanjuan et al., 2016) but is too radiogenic to indicate fluid-rock interaction with Lower Triassic sandstone. The data may indicate a mixed signal of granite and sandstone. The εNd value (−5.68) of the fluid indicates fluid-rock interaction with Lower Triassic sandstone (Sanjuan et al., 2016). The geochemistry of the Soultz fluid is similar to that of the other deep geothermal brines from granite reservoirs (Rittershoffen, Insheim, Landau, Vendenheim), but also to that of the Cronenbourg brine, which is discharged from the Lower Triassic Buntsandstein sandstone reservoir (Sanjuan et al., 2016, 2022). In general, it is assumed that the hydrothermal fluids reacted with the Lower Triassic sedimentary strata and migrated into the underlying Carboniferous granites along fractures (Dugamin et al., 2024; Sanjuan et al., 2010, 2016, 2022).

3. Samples and methods

3.1. Samples

Twenty drill core samples have been provided by Électricité de Strasbourg Géothermie (Table A.1; ÉS-Géothermie). Thin sections were prepared for all samples to characterise the paragenetic sequence and mineral textures (18 alkali feldspar-granite samples, one two-mica granite sample and one sandstone sample). Samples in which biotite-chlorite mineral pairs and feldspar-alteration phases are present were selected with the scope to characterise the main and trace element contents using electron microprobe analysis (EMPA) and laser ablation inductively coupled plasma mass spectrometry (LA-ICPMS).

3.2. Micro-XRF

A Bruker Tornado M4 micro-XRF at the Mineralogical and Geochemical Micro-Analytical Laboratory (MAGMA Lab, Department of Applied Geochemistry, Technical University of Berlin, Germany) was used to determine the qualitative element distribution and to identify macro textures in thin sections. The acceleration voltage was 50 kV using a beam current of 600 μA. For the “area” mode, the measuring point distance was 30 μm at 20 μm beam diameter and the measuring time was 60 ms per spot. The analyses were run with two simultaneously operating spectrometers in order to obtain more precise data from a stronger signal.

3.3. Electron microprobe analysis (EMPA)

The EMPA was used to determine the mineral chemistry (major element oxides) of the alteration pairs of biotite-chlorite as well as K-feldspar and plagioclase and their alteration products. The analysis was performed on polished thin sections using a JEOL-8230 microprobe in wavelength-dispersive mode at the Institute for Geosciences, University of Tübingen, Germany. For all analyses, an acceleration voltage of 15 kV and a beam current of 20 nA was used. Variable beam diameters were applied for biotite and chlorite (5 μm), feldspars (10 μm) and the altered feldspars (20 μm). For calibration, certified natural and synthetic standards (Astimex) were used (Table A.2). For the feldspars and their alteration phases, albite was used for calibration of Na, Al, and Si, plagioclase for Ca, sanidine for K, $SrTiO_3$ for Sr, and baryte for Ba. For biotite and chlorite, diopside was used for Ca, Mg and Si, Al_2O_3 for Al, sanidine for K, albite for Na, hematite for Fe, bustamite for Mn, $SrTiO_3$ for Ti, baryte for Ba and tugtupite for Cl. Hydrothermally altered feldspar is characterised by very fine-grained products yielding a dusty appearance. This was analysed completely by defocused beam as indicated by low totals (Table B.3). Data reduction was performed using the internal φ(ρz) matrix correction software of JEOL (Armstrong, 1991). In six samples, 28 EMP analyses were conducted on K-feldspar (59 in altered phases), 79 on plagioclase (51 in altered phases), 41 on biotite and 51 on chlorite. Wherever possible, the analysis was performed on grains which also contain associated alteration phases. The complete data is provided in the electronic supplement (Tables B.1–B.4).

3.4. LA-ICPMS

In-situ trace element mineral chemistry of the feldspars, biotite and their alteration products were obtained by LA-ICPMS (laser ablation inductively coupled plasma mass spectrometry). A Teledyne Analyte Excite+ ArF (193 nm) excimer laser ablation system was used, which is coupled to a Thermo-Scientific Element XR sector field mass spectrometer at the Laboratory of Environmental and Raw Materials Analysis (LERA) of the Institute of Applied Geosciences (AGW) at Karlsruhe Institute of Technology (KIT), Germany. The analyses were performed with a laser spot size of 15 μm, a pulse rate of 10 Hz and an energy density of 3.0 J/cm^2. Directly after the ablation cell, the samples were ablated in a gas stream composed of ~0.5 L/min He, 8–11 mL/min N_2 and ~0.85 L/min Ar. All analyses were performed at low oxide production rates ($UO^+/U^+ < 0.1$ %) and robust plasma conditions (sensitivity ratio $U^+/Th^+ = 1.0$). Every 24 unknown sample points, the NIST-612 glass reference material was measured to verify the collected data. The NIST-612 were also analysed for data processing and external calibration (values of Pearce et al., 1997) using the GLITTER data reduction software (GEMOC ARC National Key Centre, 2022). All signals were normalized to ^{29}Si and as an internal standard the wt.-% SiO_2 concentration of the corresponding EMPA measurement was assigned to each measuring point. BCR-2G glass was analysed to control accuracy and reproducibility. The results (Table A.3) agree with the preferred

values of the GeoReM database (Jochum et al., 2005).

In six samples, 31 LA-ICPMS analyses were conducted on K-feldspar (36 in altered phases), 70 on plagioclase (55 in altered phases), 91 on biotite and 58 on chlorite. A total of 50 trace elements were analysed, but only the trace elements Li, Rb, Sr, Cs, Ba, Zn and Pb were chosen, because of their element substitution and geochemical behaviour. The data is provided in the electronic supplement (Table B.5).

4. Granite petrography and mineral chemistry

Two granites are distinguished in the drill cores from Soultz-sous-Forêts. The two-mica granite was intersected in its roof zone (Fig. 3).

4.1. Two-mica granite

The two-mica granite is fine-grained (<1 mm), equigranular (Sou-20) and shows a typical paragenetic sequence for granite (Figs. 4, 5a). It is composed of microcline (30 ± 10 Vol-%), plagioclase (30 ± 10 Vol-%), quartz (20 ± 10 Vol-%), biotite (≤5 Vol-%), muscovite (≤5 Vol-%), with zircon and magnetite as accessories. Microcline is subhedral to euhedral with cross-hatched twin pattern, whereas plagioclase is typically anhedral with polysynthetic twinning (Fig. 5a). Quartz forms anhedral grains with undulose extinction (Fig. 5a, d). Fine-grained biotite and muscovite are anhedral and locally occur along grain boundaries of feldspar intergrown with quartz (Fig. 5e). The size of zircon and magnetite is smaller than 50 µm.

The composition of microcline is near-ideal ($K_{0.94}Na_{0.05}Al_{1.02}Si_{2.98}O_8$; Fig. 6; Table B.1A). Sodium concentrations range between 5 and 6 mol.-%. Microcline is characterised by low average concentrations of Li (~3.20 µg/g), Cs (~7.28 µg/g) and Zn (~8.39 µg/g), low to moderate Pb (~139 µg/g) content, moderate concentrations of Rb (~473 µg/g), Sr (~337 µg/g), and high concentrations of Ba (~2395 µg/g) (Table B.6A, Fig. 7a, b).

Plagioclase is oligoclase in the core ($\phi Ca_{0.17}Na_{0.83}K_{0.01}Al_{1.18}Si_{2.82}O_8$) and albite in rims ($\phi Na_{0.98}K_{0.02}Al_{1.03}Si_{2.98}O_8$) and patchy zones (Table B.1B, Fig. 6). Core and rim have low average concentrations of Li (~5.00 µg/g), Cs (~7.95 µg/g) and Zn (9.90 µg/g), low to moderate concentration of Pb (~141 µg/g), moderate concentrations of Rb (~504 µg/g) and Sr (~355 µg/g) and high concentrations of Ba (~2574 µg/g) (Table B.6, Fig. 7a, b).

Biotite plots slightly away from the ideal mixing line between annite and phlogopite at approx. Phl_{37} (Fig. 8). It is rich in Fe (23.1 wt.-% FeO_{tot}) and Ti (3.06 wt.-% TiO_2) (Table B.2A). Magnesium is substituted by Al on the tetrahedral site, which results in the composition

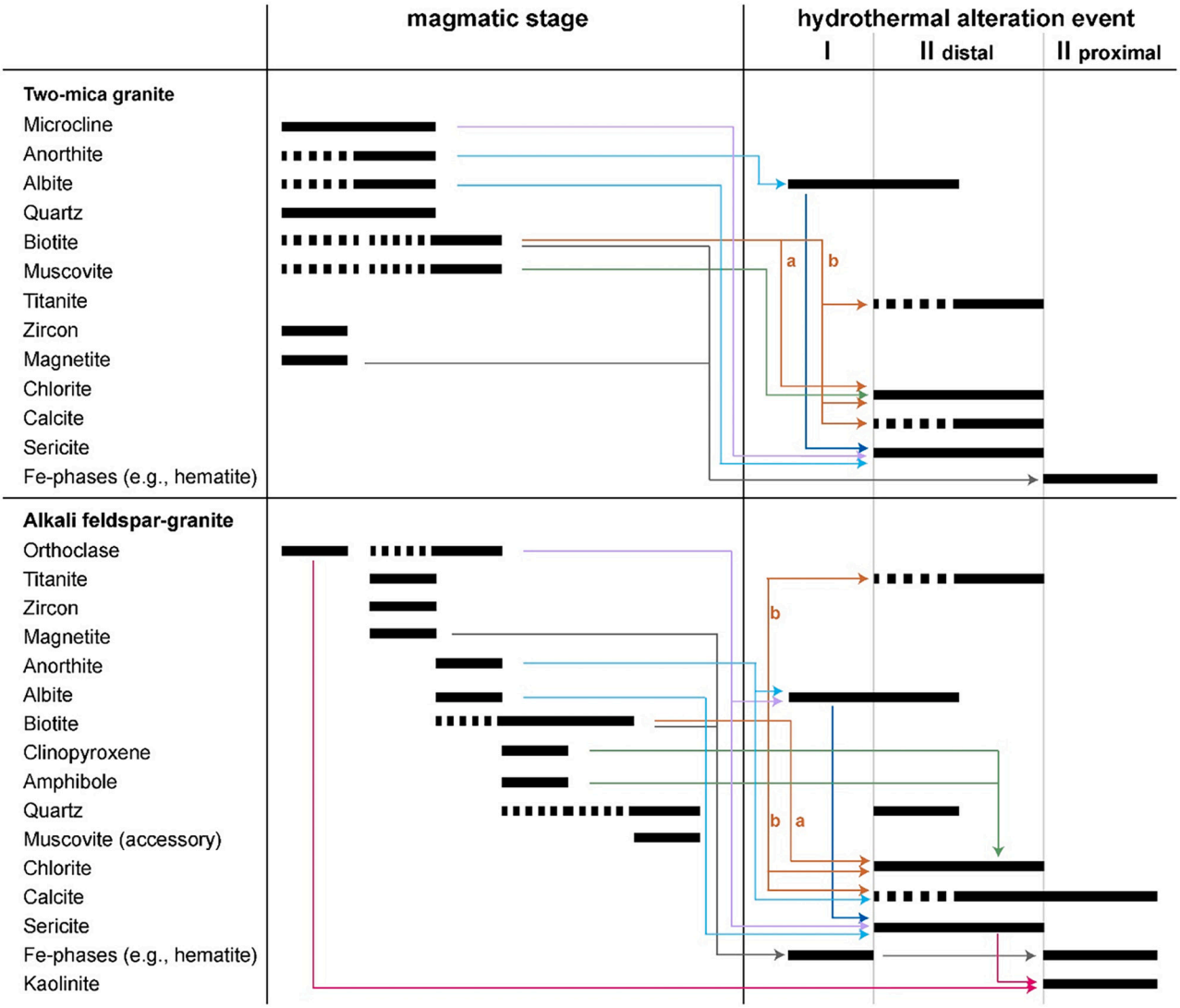

Fig. 4. Paragenetic sequence of the two-mica granite (Sou-20) and alkali feldspar-granite (Sou-4,7,12,14,19). Sericite indicates a mixture of fine-grained muscovite and illite. Alteration processes are indicated by arrows. Event II distal and proximal replacement to hydrothermal veins.

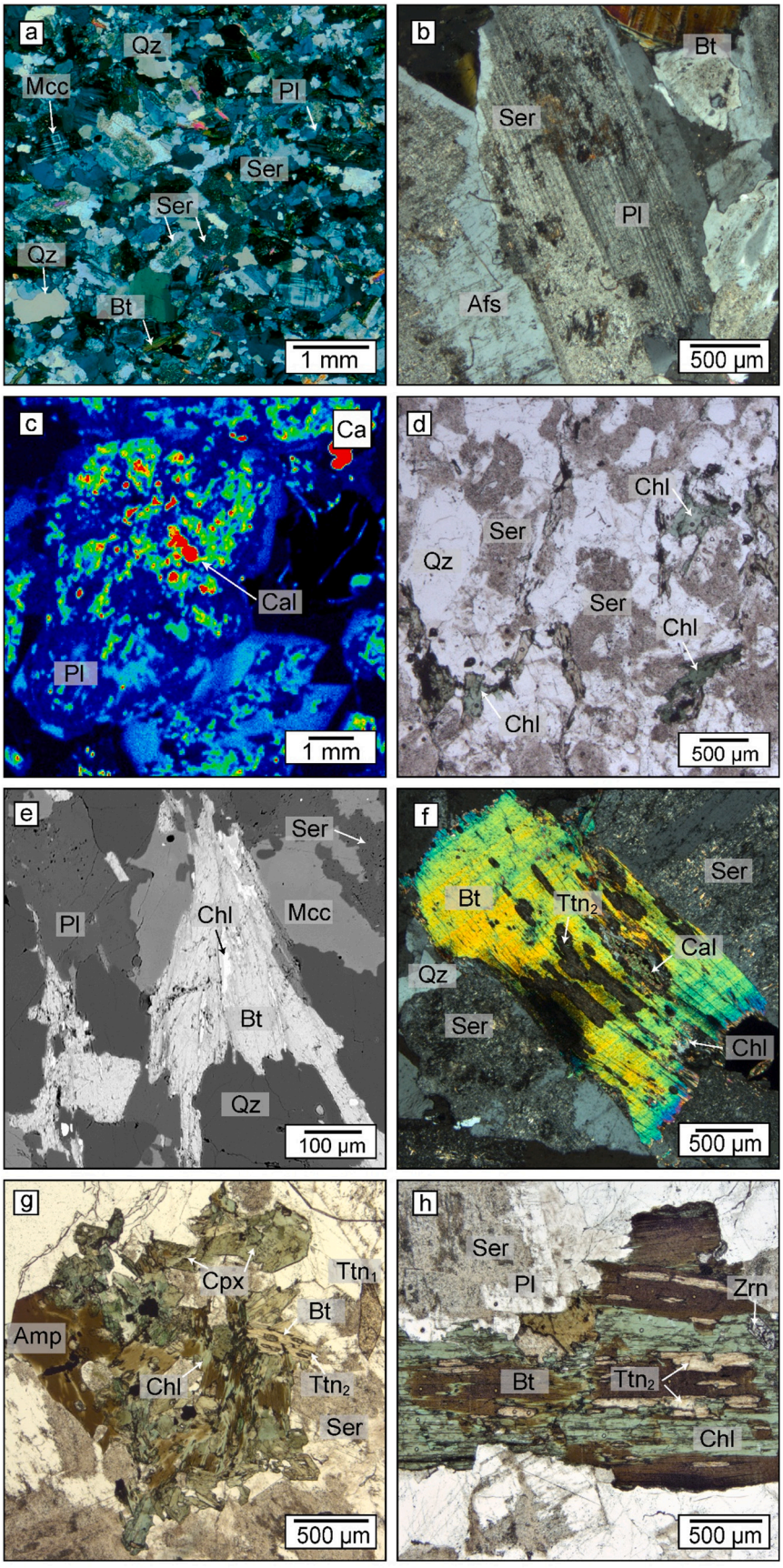

(caption on next page)

Fig. 5. Photomicrographs (a–h) and Micro-XRF element map (c) of the two-mica granite and alkali feldspar-granite showing the magmatic assemblage, the event 1 albitization and weak event 2 hydrothermal alteration: (a) The typical magmatic microcline, plagioclase, biotite and quartz assemblage (Sou-20, two-mica granite). Note intense hydrothermal event 2 sericite dusting in feldspar cores that is less intense in event 1 albite rims. (b) Microphotograph showing alkali feldspar and plagioclase altered to sericite (Sou-14, alkali feldspar-granite). Note the less intense event 2 sericitization of the event 1 albite rims, indicating that hydrothermal albite is replaced by sericite, but hydrothermal alteration intensity depends on host mineral composition. (c) Plagioclase shows patchy, Ca-rich zones in the cores, indicating event 1 albitization mainly at the rims. Very high Ca-contents (red colours) correlate with event 2 calcite alteration (Sou-4, alkali feldspar-granite). Hydrothermal event 2 alteration: (d) Feldspars are intensely replaced by sericite, whereas biotite is completely replaced by chlorite (Sou-20, two-mica granite). Note the hydrothermal quartz. (e) Back scattered image showing chlorite replacing biotite along cleavage planes (Sou-20, two-mica granite). (f) Sericitization and biotite replaced by chlorite, titanite and calcite (Sou-4, alkali feldspar-granite). (g) Mineral aggregates of amphibole, biotite, clinopyroxene and euhedral titanite with replaced by chlorite and titanite (Sou-12, alkali feldspar-granite). (h) Hydrothermal alteration of plagioclase and biotite to sericite, and chlorite and titanite, respectively (Sou-7, alkali feldspar-granite). Abbreviations after Warr (2020, 2021): Afs alkali feldspar, Amp amphibole, Bt biotite, Cal calcite, Chl chlorite, Cpx clinopyroxene, Mcc microcline, Pl plagioclase, Qz quartz, Ser sericite, Ttn titanite, Zrn zircon. (For interpretation of the references to colour in this figure legend, the reader is referred to the web version of this article.)

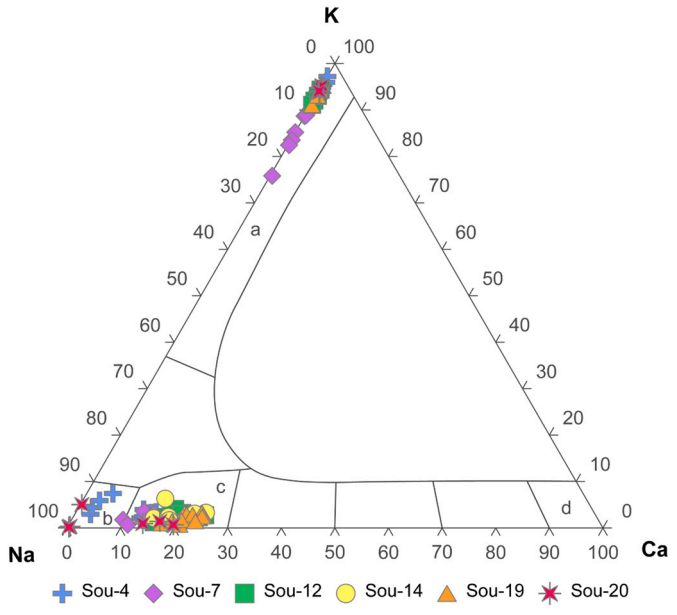

Fig. 6. Composition of K-feldspar and plagioclase in the two-mica granite (Sou-20) and the alkali feldspar-granite (Sou-4 to Sou-19) in apfu represented in molar percentage. Formula re-calculated to 16 cation charges, 5 cations, and 8 O (n = 28 Kfs, n = 79 Pl). Isotherms at 900 °C and 0.5 kbar (after Deer et al. (2001)) a:sanidine with endmember orthoclase/microcline, b: albite, c: oligoclase, d: anorthite.

$K_{0.98}Na_{0.01}\left[Fe^{2+}_{1.11}Mg_{0.91}Mn_{0.02}Al_{0.34}Ti_{0.18}\right]Al_{1.18}Si_{2.82}O_{10}Cl_{0.01}(OH)_2$. Biotite has low average concentrations of Cs (~38.8 µg/g), Sr (~3.39 µg/g) and Pb (~6.55 µg/g), moderate concentrations of Zn (528 µg/g), moderate to high contents of Li (~650 µg/g), and high concentrations of Rb (~1148 µg/g) and Ba (~3477 µg/g) (Table B.6A, Fig. 7a, b).

Muscovite contains additional Fe (5.64–6.06 wt.-% FeO_{tot}), Ti (0.36–2.13 wt.-% TiO_2) and Mg (0.95–2.11 wt.-% MgO) (Table B.2B). It has low average concentrations of Cs (~106 µg/g), Sr (~5.76 µg/g), Pb (~11.8 µg/g) and high concentrations of Li (~1291 µg/g), Rb (~2461 µg/g), Ba (~4328 µg/g) and Zn (~992 µg/g) (Table B.6A, Fig. 7a, b).

4.2. Alkali feldspar-granite

The alkali feldspar-granite (Sou-4, Sou-7, Sou-12, Sou-14, Sou-19) consists of reddish K-feldspar phenocrysts in a coarse-grained, equigranular texture of K-feldspar (30 ± 10 Vol-%), plagioclase (20 ± 10 Vol-%), quartz (40 ± 10 Vol-%) and biotite (5 Vol-%) (Figs. 4, 5b). Accessory minerals (≤5 Vol-%) are titanite, zircon, clinopyroxene, amphibole, magnetite and muscovite. The reddish tabular K-feldspar phenocrysts (2–5 cm) are euhedral, partly subhedral with Carlsbad twins. They are locally (Sou-19) fractured and have fine-grained, anhedral quartz inclusions. Locally perthitic exsolution lamellae are observed in the phenocrysts and the smaller, subhedral to locally euhedral orthoclase (~2 cm) in paragenesis. The K-feldspar is accompanied by equigranular, lath-shaped, subhedral plagioclase (~2 cm) with polysynthetic twinning (Fig. 5b). The plagioclase has albite rims and locally patchy albite zones (Fig. 5b, c). Anhedral quartz (≤2 cm) is fine- to medium-grained and shows undulose extinction. Biotite is present as subhedral flakes (≤2 cm) with characteristic cleavage (Fig. 5f, h). Titanite (≤1 mm), zircon (≤50 µm) and magnetite (≤200 µm) are often euhedral and associated or included within biotite, clinopyroxene or amphibole (Fig. 5g, h). Biotite, clinopyroxene and amphibole form mineral aggregates.

Tabular K-feldspar phenocrysts of Sou-19 have a near-ideal K-feldspar composition ($K_{0.96}Na_{0.04}AlSi_3O_8$) with a small amount of Fe (<0.12 wt.-% FeO_{tot}) (Fig. 6; Table B.1A). They have low average concentrations of Li (~1.69 µg/g), Cs (~2.00 µg/g), Zn (11.2 µg/g) and Pb (62.5 µg/g), moderate concentrations of Rb (~349 µg/g), and moderate to high concentrations for Sr (846 µg/g) and Ba (3441 µg/g) (Sou-19; Table B.6B, Fig. 7a, b).

The fine-grained orthoclase (Sou-4 to Sou-14) has a near-ideal K-feldspar composition ($K_{0.95}Na_{0.05}AlSi_3O_8$) with a small amount of Fe (<0.19 wt.-% FeO_{tot}) (Fig. 6; Table B.1A). Sodium concentration ranges between b.d.l.-25 mol-% and mainly 5–10 mol-% (Fig. 6). The matrix orthoclase has low average concentrations of Li (~2.35 µg/g), Rb (~44.4 µg/g), Cs (~1.67 µg/g), Ba (~90 µg/g), Zn (~4.24 µg/g), and Pb (~30.7 µg/g) and moderate to high average concentrations of Sr (~597 µg/g) (Table B.6B, Fig. 7a, b).

Plagioclase is oligoclase ($Ca_{0.23}Na_{0.75}K_{0.03}Al_{1.24}Si_{2.77}O_8$) in the core and albite at rims and in patches (Fig. 7a; $Na_{0.9}K_{0.06}Ca_{0.03}Al_{1.12}Si_{2.91}O_8$). Both have a small amount of K (<10 mol.-%) and Fe (<0.24 wt.-% FeO_{tot}) (Table B.1B, Fig. 6). They have similar low average concentrations of Li (~2.90 µg/g), Rb (~3.93 µg/g), Cs (~0.198 µg/g), Ba (~65.6 µg/g), Zn (~4.17 µg/g) and Pb (~29.3 µg/g) and moderate to high concentrations of Sr (~645 µg/g) (Table B.6B, Fig. 7a, b).

Biotite is a near-ideal solid solution of the endmembers annite and phlogopite Phl_{55-63} (Fig. 8). It has a uniform composition (Table B.2A) with low concentrations of Ti (1.49–3.81 wt.-% TiO_2), Mn (0.43–0.94 wt.-% MnO), Ba (0.06–0.44 wt.-% BaO) and Na (0.07–0.23 wt.-% Na_2O) (Table B.2A). It has low average concentrations of Cs (~42.5 µg/g), Sr (~3.51 µg/g) and Pb (~2.44 µg/g), moderate Li (~490 µg/g) and Zn (~481 µg/g) concentrations, and high average concentrations of Rb (~920 µg/g) and Ba (~850 µg/g) (Table B.6B, Fig. 7a, b).

5. Hydrothermal alteration

Two hydrothermal alteration events are distinguished. The first event is the albitization of K-feldspar and plagioclase. The second event is the hydrothermal alteration of the feldspars to sericite (mixed aggregates of muscovite and illite), and the alteration of biotite to chlorite. This second event is correlated with the pervasive alteration type (Genter et al., 1997). Proximal to veins and abundant cracks, the second hydrothermal stage contains kaolinite. This is correlated with the vein alteration (Genter et al., 1997).

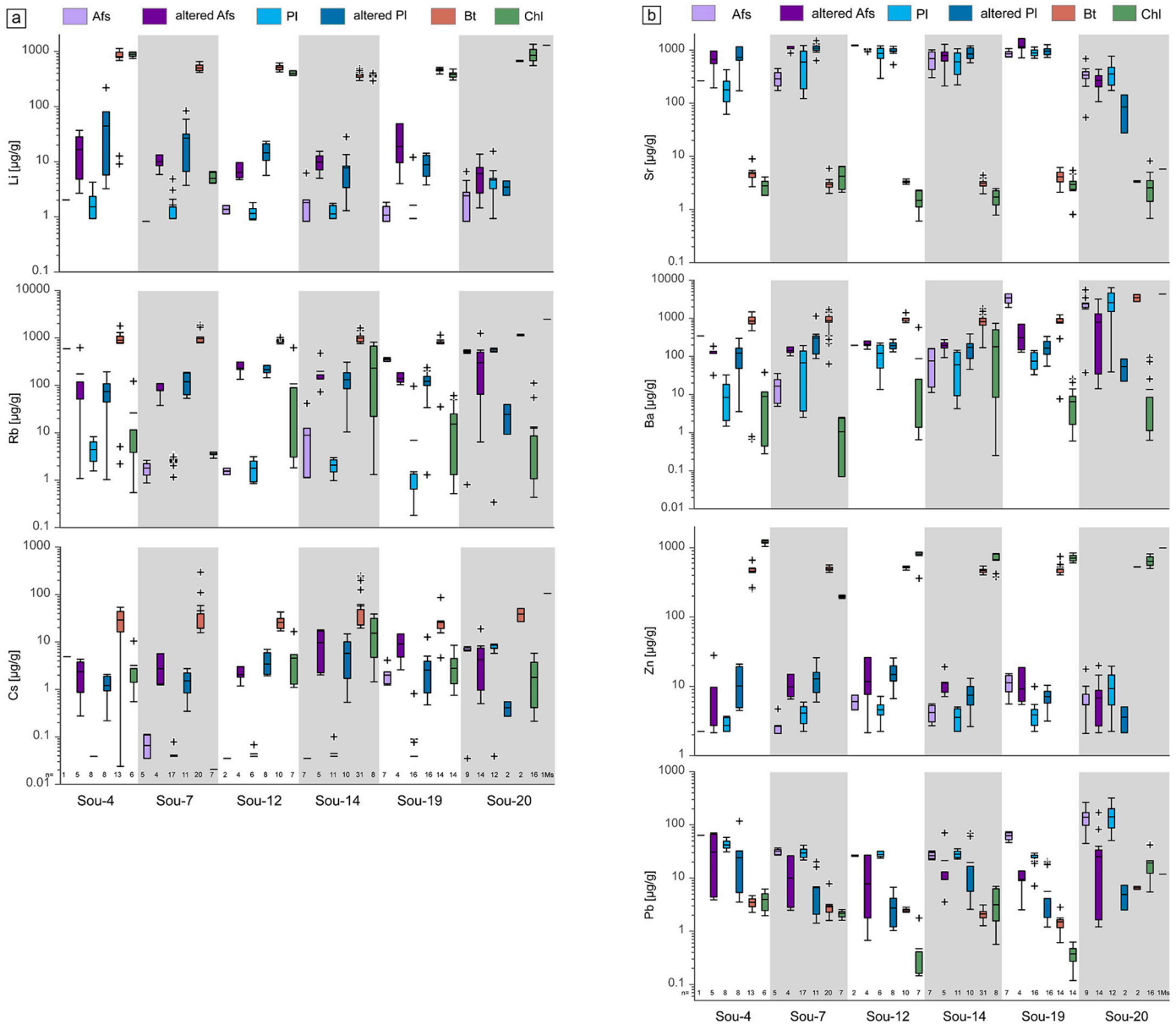

Fig. 7. Boxplots illustrating the mineral trace element composition sorted after sample and element. The order of the minerals corresponds to the order of the legend. a) alkaline elements, b) alkaline earth elements and Pb, Zn. Boxplots represent mean, lower (0.25-quantile) and upper quartile (0.75-quantile), lower and upper whisker and outliers (minimum and maximum values). Data below detection limit are included with the value of the calculated detection limit (Table B; method of fixed-value imputation adapted from Frenzel (2023)).

5.1. Event 1: albitization

Plagioclase in the two-mica and alkali feldspar-granite have thin albite rims and locally patchy albite zones in their cores (Fig. 5b). The albite rims are recognized by different extinction behaviour and less intense sericitization in hydrothermally altered samples (Fig. 9e). Furthermore, micro-XRF maps show Ca-enriched cores, patchy Ca-depleted zones and Ca-poor rims in plagioclase (Fig. 5c). Trace elements in oligoclase, K-feldspar and albite alteration zones do not differ significantly, indicating that this hydrothermal alteration event 1 did not involve major geochemical changes.

5.2. Event 2: hydrothermal chlorite-sericite-(kaolinite) alteration

The hydrothermal chlorite-sericite assemblage in both granites is additionally characterised by titanite, calcite and hematite (Figs. 4, 5f–h). All feldspars, including their albite rims and patches, are replaced by sericite and calcite predominantly in the Ca-rich cores and along grain boundaries (Fig. 5b, c), indicating that hydrothermal chlorite-sericite alteration postdates albitization. Sericite is more abundant replacing plagioclase rather than K-feldspar (Figs. 5a, b, d, f, 9a). Muscovite and biotite are replaced by chlorite along grain boundaries and cleavage planes (Figs. 5e–h, 9b, c). Domains in biotite that are more frequently replaced by chlorite typically contain anhedral titanite and calcite in assemblage with chlorite (Figs. 5f–h, 9b, c). Also, accessory clinopyroxene and amphibole are weakly replaced by chlorite along grain boundaries and rims (Fig. 5g).

Proximal to hydrothermal quartz-baryte-galena veins in granite (Sou-8, 13, 15) are strongly altered and no primary minerals except local biotite are recognized (Fig. 10a, b). This means that the hydrothermal alteration event 2 is correlated either to the Middle Jurassic-Cretaceous or the Cenozoic vein events in the Black Forest (Burisch et al., 2018;

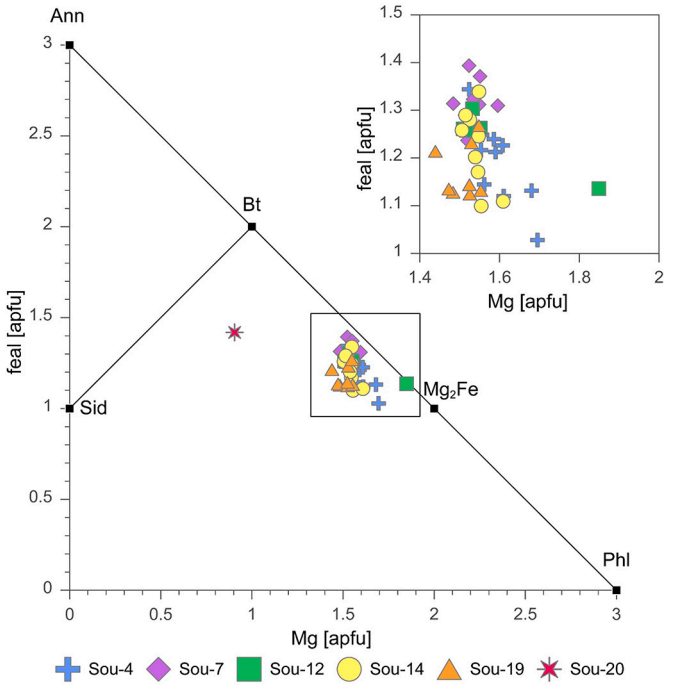

Fig. 8. Biotite composition of the two-mica granite (Sou-20) and the alkali feldspar-granite (Sou-4 to Sou-19) in apfu. Formula recalculated to 22-cation charges, 8 cations, and 11 O (n = 41) based on Tischendorf et al. (2004) (feal [apfu] = Fe_{tot} + Mn + Ti − ^{VI}Al).

Walter et al., 2018b). In particular, the alkali feldspar-granite is crosscut by calcite veins that are surrounded by a calcite-kaolinite-hematite alteration zone (Fig. 10c, d). Biotite, plagioclase and orthoclase in the matrix are replaced by calcite and kaolinite. Orthoclase phenocrysts are replaced by hematite and other Fe-phases (Fig. 10a). Matrix K-feldspar and plagioclase are completely altered to sericite, kaolinite and calcite (Fig. 10b, d). Secondary, hydrothermal quartz fills cracks in K-feldspar phenocrysts which are, in addition, locally filled by calcite (Fig. 10c, d).

The alteration product of K-feldspar in general has increased Na, Ca and decreased K contents (Table B.3A, Fig. 11). In the two-mica granite, they have low average concentrations of Li (~6.05 μg/g), Cs (~4.26 μg/g), Zn (~7.17 μg/g) and Pb (~25.2 μg/g), moderate Rb (~303 μg/g) and Sr (~269 μg/g) contents, and moderate to high average concentrations of Ba (~789 μg/g). In the alkali feldspar-granite, they have low average concentrations of Li (~12.4 μg/g), Cs (~5.27 μg/g), Zn (~11.1 μg/g) and Pb (~16.7 μg/g), low to moderate Ba (~191 μg/g) and Rb (~166 μg/g) concentrations, and high concentrations of Sr (~916 μg/g) (Table B.6A, Fig. 7a, b). Alteration of plagioclase shows an increase in Ca and K compared to least altered plagioclase, while the Na-content decreases (Table B.3B, Fig. 11). The trace elements in the alteration products of plagioclase in the two-mica granite have low average concentrations of Li (~3.47 μg/g), Rb (~24.3 μg/g), Cs (~0.41 μg/g), Sr (~85.3 μg/g), Ba (~54.0 μg/g), Zn (~5.04 μg/g) and Pb (~4.92 μg/g). In the alteration products of plagioclase in the alkali-feldspar-granite, the average concentrations are low for Li (~18.5 μg/g), Cs (~2.87 μg/g), Zn (~9.97 μg/g) and Pb (~10.8 μg/g), low to moderate for Rb (~130 μg/g), Ba (~193 μg/g), and high for Sr (~924 μg/g) (Table B.6A, Fig. 7a, b). The major element distribution of increased Na, K and Ca is in accordance with sericite-calcite replacement that is observed petrographically and also supported by trace element enrichment of Li, Rb, Cs and Sr, which are incorporated into the alteration assemblage.

The Si-content in chlorite ranges between 2.7 and 3.4 apfu, proportional to variations in the Al content (Table B.4, Fig. 12). Iron-rich chlorite (chamosite) is exclusively hosted in two-mica granite (Table B.4, Fig. 12). Chamosite has low average concentrations of Rb (~13.2 μg/g), Cs (~1.79 μg/g), Sr (~2.57 μg/g), Ba (~13.6 μg/g) and Pb (~19.2 μg/g), moderate average Zn content (~636 μg/g) and moderate to high Li concentrations (~851 μg/g). Chlorite of the alkali feldspar-granite is clinochlore (Table B.4, Fig. 12). It has low concentrations of Rb (~71.3 μg/g), Cs (~6.07 μg/g), Sr (~2.67 μg/g), Ba (~55.0 μg/g) and Pb (~1.73 μg/g), a moderate average Li concentrations (~390 μg/g), except sample Sou-7 (~4.97 μg/g) and high Zn concentrations (~693 μg/g) except for Sou-7 (~195 μg/g) (Table B.6B, Fig. 7a, b).

5.3. Hydrothermal mineral reactions and element mobility

Since we cannot conclusively distinguish between muscovite and illite in the complex and fine-grained sericite intergrowth of the hydrothermal alteration event 2, we look at reactions involving both minerals as components, separately (Eqs. (1)–(4) and (5)–(8)). The hydrothermal alteration of the anorthite component to muscovite consumes 4 mol K and no ions are released to the fluid (Eq. (1)). In comparison, the same reaction with the oligoclase component consumes 4 mol K but releases 6 mol Na (Eq. (2)). Silica and Ca are released during the reactions, which explains hydrothermal quartz and calcite growth in the altered samples (Fig. 9a).

$$3CaAl_2Si_2O_8 + 3CO_2 + 2K^+ + 3H_2O \longrightarrow 2KAl_3Si_3O_{10}(OH)_2 + 3CaCO_3 + 2H^+ \quad (1)$$

$$3Na_2CaAl_4Si_8O_{24} + 3CO_2 + 4K^+ + 2H^+ + 3H_2O \longrightarrow 4KAl_3Si_3O_{10}(OH)_2 + 3CaCO_3 + 12SiO_2 + 6Na^+ \quad (2)$$

The hydrothermal alteration of albite and K-feldspar to muscovite releases 3 mol Na and 2 mol K, respectively (Eqs. (3), (4)). One mole K is consumed by the hydrothermal alteration of albite (Eq. (4)). Silica is also released by the alteration of alkali feldspar, which is shown by hydrothermal quartz in cracks (Fig. 10d).

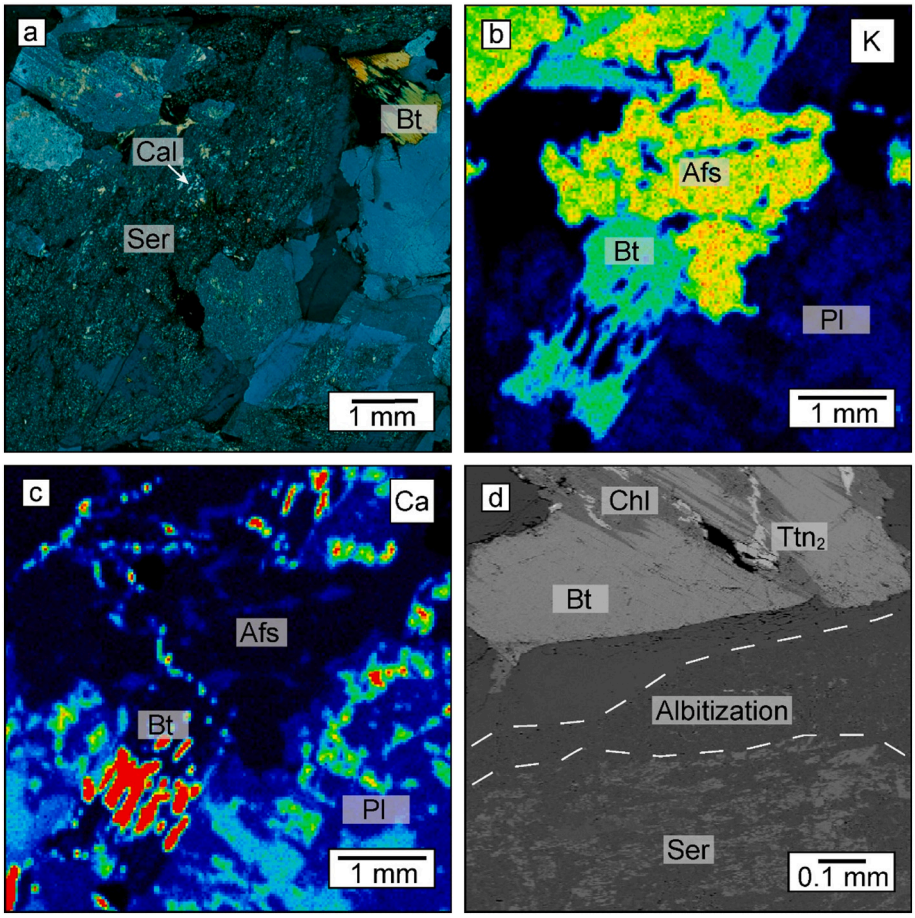

Fig. 9. Plagioclase and biotite in alkali feldspar-granite (Sou-4). (a) Microphotograph of event 2 sericite-calcite replacement of plagioclase. (b, c) Micro-XRF element maps: biotite shows K-poor and Ca-rich patches indicating replacement by titanite along cleavage planes during hydrothermal alteration event 2. (d) BSE image: event 1 albite rim in plagioclase and event 2 sericitization and replacement of biotite by chlorite along cleavage plains. Colours in (b, c): light blue: low concentration, greenish: intermediate concentration, red: highest concentration. Abbreviations after Warr (2020, 2021): Afs alkali feldspar, Bt biotite, Cal calcite, Chl chlorite, Pl plagioclase, Qz quartz, Ser sericite, Ttn titanite. (For interpretation of the references to colour in this figure legend, the reader is referred to the web version of this article.)

$$3NaAlSi_3O_8 + K^+ + 2H^+ \longrightarrow KAl_3Si_3O_{10}(OH)_2 + 6SiO_2 + 3Na^+ \quad (3)$$

$$3KAlSi_3O_8 + 2H^+ \longrightarrow KAl_3Si_3O_{10}(OH)_2 + 6SiO_2 + 2K^+ \quad (4)$$

The respective reactions to illite (Eqs. (5)–(8)) are very similar. The hydrothermal alteration to illite consumes less K and Na is quantitatively released, whereas Ca is immobilized in calcite if CO_2 is present. Released SiO_2 forms hydrothermal quartz. Most of the reactions consume H^+ and are thus favourable under slightly acidic conditions.

$$3KAlSi_3O_8 + 2.15\text{-}2.40H^+ + 0.0375\text{-}0.1O_2 \longrightarrow K_{0.60\text{-}0.85}Al_3Si_3O_{10}(OH)_2 + 6SiO_2 + 2.15\text{-}2.40K^+ + 0.075\text{-}0.2H_2O \quad (5)$$

$$3NaAlSi_3O_8 + 0.60\text{-}0.85K^+ + 2.15\text{-}2.40H^+ + 0.0375\text{-}0.1O_2 \longrightarrow K_{0.60\text{-}0.85}Al_3Si_3O_{10}(OH)_2 + 6SiO_2 + 3Na^+ + 0.075\text{-}0.2H_2O \quad (6)$$

$$3Na_2CaAl_4Si_8O_{24} + 3CO_2 + 2.4\text{-}3.4K^+ + 2.6\text{-}3.6H^+ + 3H_2O + 0.3\text{-}0.8O_2 \longrightarrow 4K_{0.60\text{-}0.85}Al_3Si_3O_{10}(OH)_2 + 3CaCO_3 + 12SiO_2 + 6Na^+ + 0.3\text{-}0.8H_2O \quad (7)$$

$$3CaAl_2Si_2O_8 + 3CO_2 + 1.2\text{-}1.7K^+ + 3H_2O + 0.075\text{-}0.2O_2 \longrightarrow 2K_{0.60\text{-}0.85}Al_3Si_3O_{10}(OH)_2 + 3CaCO_3 + 1.2\text{-}1.7H^+ + 0.15\text{-}0.40H_2O \quad (8)$$

In the event 2 hydrothermal reactions of biotite to chlorite and additional titanite and calcite (Fig. 5f, h), K, Mg, Fe and SiO_2 are released, while Ca from plagioclase and Ti from biotite are consumed (Eqs. (9), (10)). Protons are either consumed or released, indicating pH-dependence of the reactions.

$$2K(Mg,Fe)_3AlSi_3O_{10}(OH)_2 + 4H^+ \longrightarrow (Mg,Fe)_5Al_2Si_3O_{10}(OH)_8 + 2K^+ + (Mg,Fe)^{2+} + 3SiO_2 \quad (9)$$

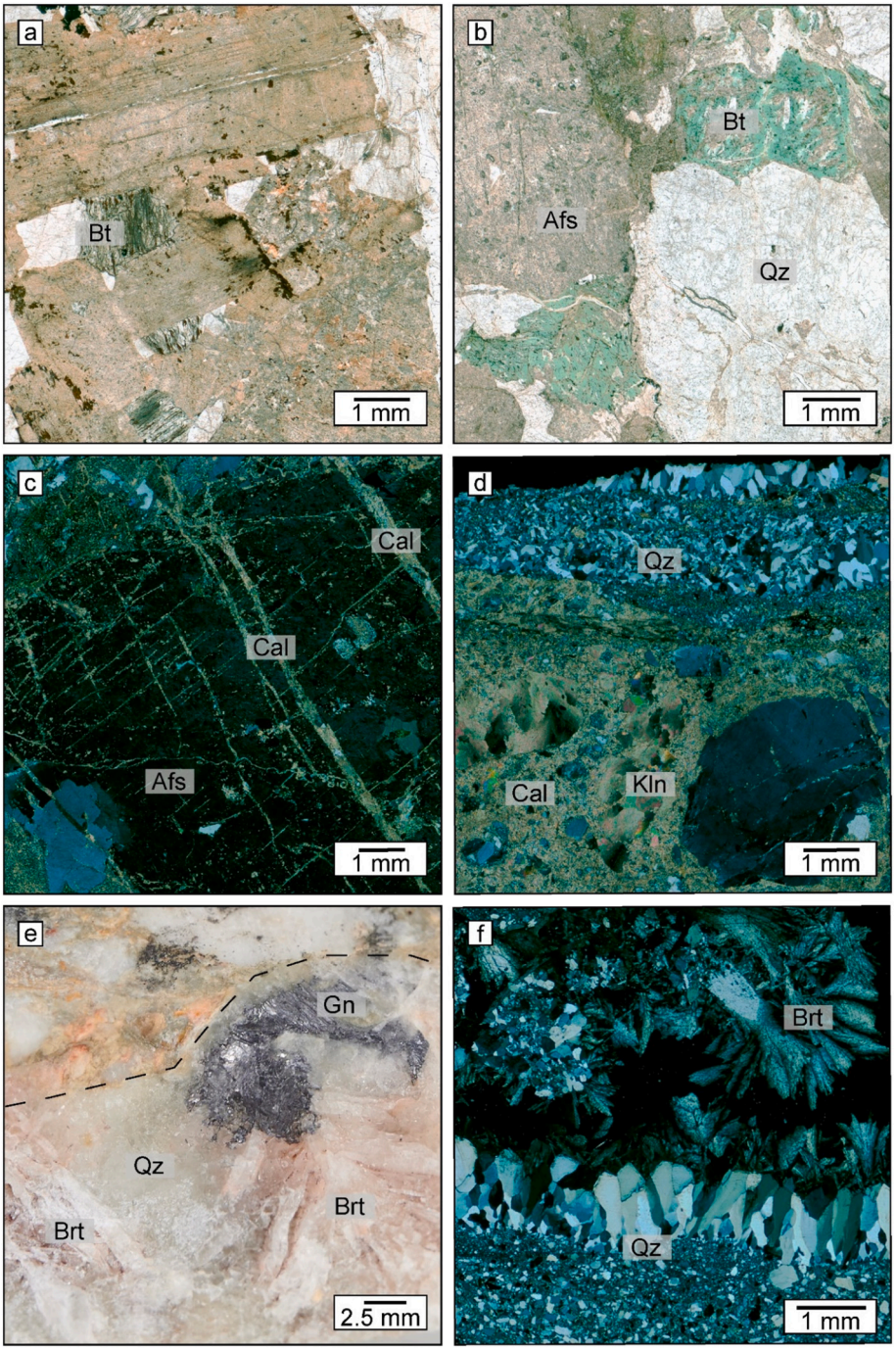

Fig. 10. Microphotographs of intensely altered alkali feldspar-granite (proximal event 2). (a) Completely altered feldspar and biotite (Sou-13). (b) Completely altered alkali feldspar phenocryst and biotite altered to chlorite (Sou-15). Note that the crystal shape is preserved. (c) Alkali feldspar phenocryst with cracks filled by calcite (Sou-15). (d, e) Quartz-baryte vein with proximal hydrothermal alteration in alkali feldspar-granite of Sou-8. (f) Quartz-baryte vein with galena in sandstone (Sou-1). Abbreviations after Warr (2020, 2021): Afs alkali feldspar, Brt baryte, Bt biotite, Cal calcite, Chl chlorite, Gn galenite, Kln kaolinite, Qz quartz.

$$2K(Mg,Fe)_3AlSi_3O_{10}(OH)_2 + 2Ca^{2+} + Ti^{4+} + 4H_2O + CO_2 \longrightarrow (Mg,Fe)_5Al_2Si_3O_{10}(OH)_8 + CaTiSiO_5 + CaCO_3 + 2K^+ + (Mg,Fe)^{2+} + 2SiO_2 + 4H^+ \quad (10)$$

Assuming that the monovalent ions Li, Rb and Cs behave similarly to K and Na, these elements can also be released during the described hydrothermal reactions of biotite and the feldspars. However, since Li, Rb and Cs may also be incorporated in the K-site of muscovite or illite, they likely are directly consumed in the reaction and not transferred to the fluid. The sericite from altered feldspars has slightly higher Li or very similar concentrations than the parent mineral supporting this interpretation (Fig. 7a). Similarly, chlorite has similar or even higher Li-

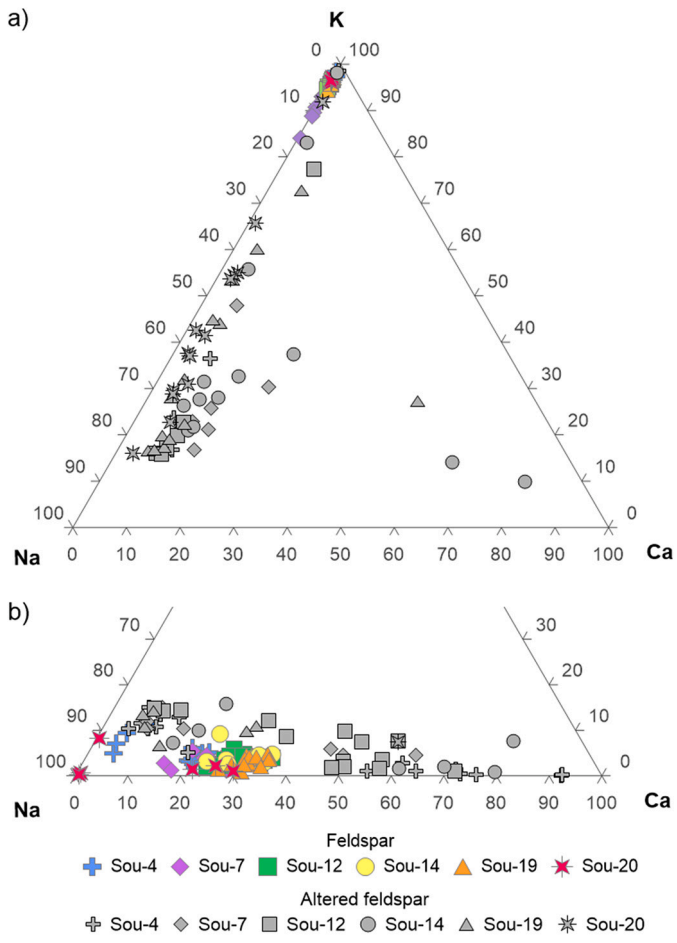

Fig. 11. EMPA data of a) altered alkali feldspar (n = 59) and b) altered plagioclase (n = 51) compared to their non-altered phases in wt.-%.

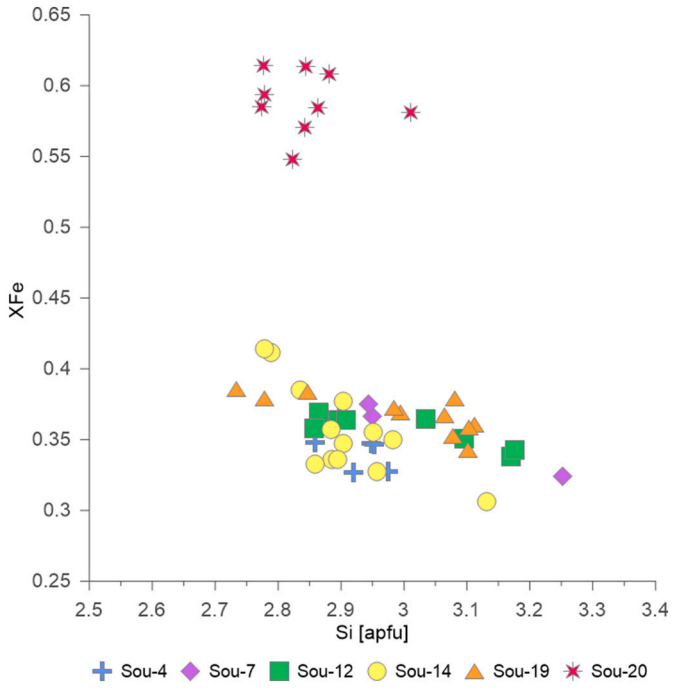

Fig. 12. Chlorite composition in the two-mica granite (Sou-20) and the alkali feldspar-granite (Sou-4 to Sou-19) in apfu. Formula recalculated to 28 cation charges, 10 cations, and 14 O (n = 51). XFe = $Fe_{tot}/(Fe_{tot} + Mg + Mn)$.

concentrations than biotite (Table B.5, Fig. 7a). A simplified comparison of the compositional data, however, does not take mass balance into account.

Along cracks, K-feldspar and sericite are hydrothermally altered to kaolinite during proximal event 2 under acidic conditions and reduced K^+ and SiO_2 activity (Eqs. (11), (12); Fig. 10d). The latter are released to the fluid during the reaction.

Furthermore, also at high fluid-rock ratio, acidic pH and steady-state conditions, K-feldspar reacts to kaolinite and quartz releasing K^+ (Eq. (11)). Low fluid-rock ratios result in an enrichment of K^+ in the fluid, and kaolinite and feldspar react to illite/muscovite (Eq. (13)) (Bjørkum and Gjelsvik, 1988; Yuan et al., 2019).

$$KAl_3Si_3O_{10}(OH)_2 + K_{0.60\text{-}0.85}Al_3Si_3O_{10}(OH)_2 + 2H^+ + 3H_2O \longrightarrow Al_2Si_2O_5(OH)_4 + 2\text{-}xK^+ \quad (11)$$

$$KAlSi_3O_8 + 2H^+ + H_2O \longrightarrow Al_2Si_2O_5(OH)_4 + 4SiO_2 + 2K^+ \quad (12)$$

$$Al_2Si_2O_5(OH)_4 + KAlSi_3O_8 \longrightarrow KAl_3Si_3O_{10}(OH)_2 + 2SiO_2 + H_2O \quad (13)$$

6. Mass balance calculation

Mass balance is calculated for major and selected trace elements using the isocon method after Grant (1986, 2005). The isocon method is sensitive to analytical error, sample heterogeneity and hydrothermal alteration (Grant, 2005). By applying the isocon method to the mineral major and trace element data, all other effects are excluded except for the dependence on analytical uncertainty. By plotting the trace element concentration of the alteration pairs, conclusions can be made about the immobility ($\Delta c_i = 0$), gain ($\Delta c_i > 0$) and loss ($-1 < \Delta c_i < 0$) in the mineral system (Eq. (14)).

$$\frac{\Delta c_i}{c_i^O} = \left(\frac{c^O_{Al_2O_3}}{c^A_{Al_2O_3}}\right)\left(\frac{c_i^A}{c_i^O}\right) - 1 = \frac{1}{S}\left(\frac{c_i^A}{c_i^O}\right) - 1 \rightarrow \Delta c_i = \left[\frac{1}{S}\left(\frac{c_i^A}{c_i^O}\right) - 1\right] c_i^O \quad (14)$$

$$\Delta m = \left[\frac{1}{S} - 1\right] * 100\% \quad (15)$$

$$\Delta V = \left[\frac{1}{S}\left(\frac{\rho^A}{\rho^O}\right) - 1\right] * 100\% \quad (16)$$

Δc_i change in concentration of species i
c_i^O concentration of species i in the precursor
c_i^A concentration of species i in the alteration product
$c^O_{Al_2O_3}$, $c^A_{Al_2O_3}$ concentration of the immobile species Al
S slope of the isocon
Δm, ΔV mass and volume change
ρ^O, ρ^A specific densities of the minerals

We use the mean of the major and trace element data (Tables B.1–B.4, B.6) and assume that Al is immobile during hydrothermal alteration, which is supported by the balanced mineral reactions.

Hydrothermal alteration of K-feldspar in both granites causes enrichment of Fe, Ca, Na, Li and V in the event 2 hydrothermal alteration assemblage (Fig. 13; cf. Figs. A.1, A.2, Table C.1). Silica, K, Ba and Pb are generally depleted, and the rest of the elements remain immobile (Fig. 13, Figs. A.1, A.2). Only Cs appears to behave differently in the two granites (Figs. 13, Figs. A.1, A.2). Mass and volume loss related to the mineral reactions are ~25 % and ~20 %, respectively. Plagioclase alteration is related to Fe-, V- and K-enrichment in the hydrothermal alteration product, whereas Pb is depleted, and Si, Al, Na, Ni and Co

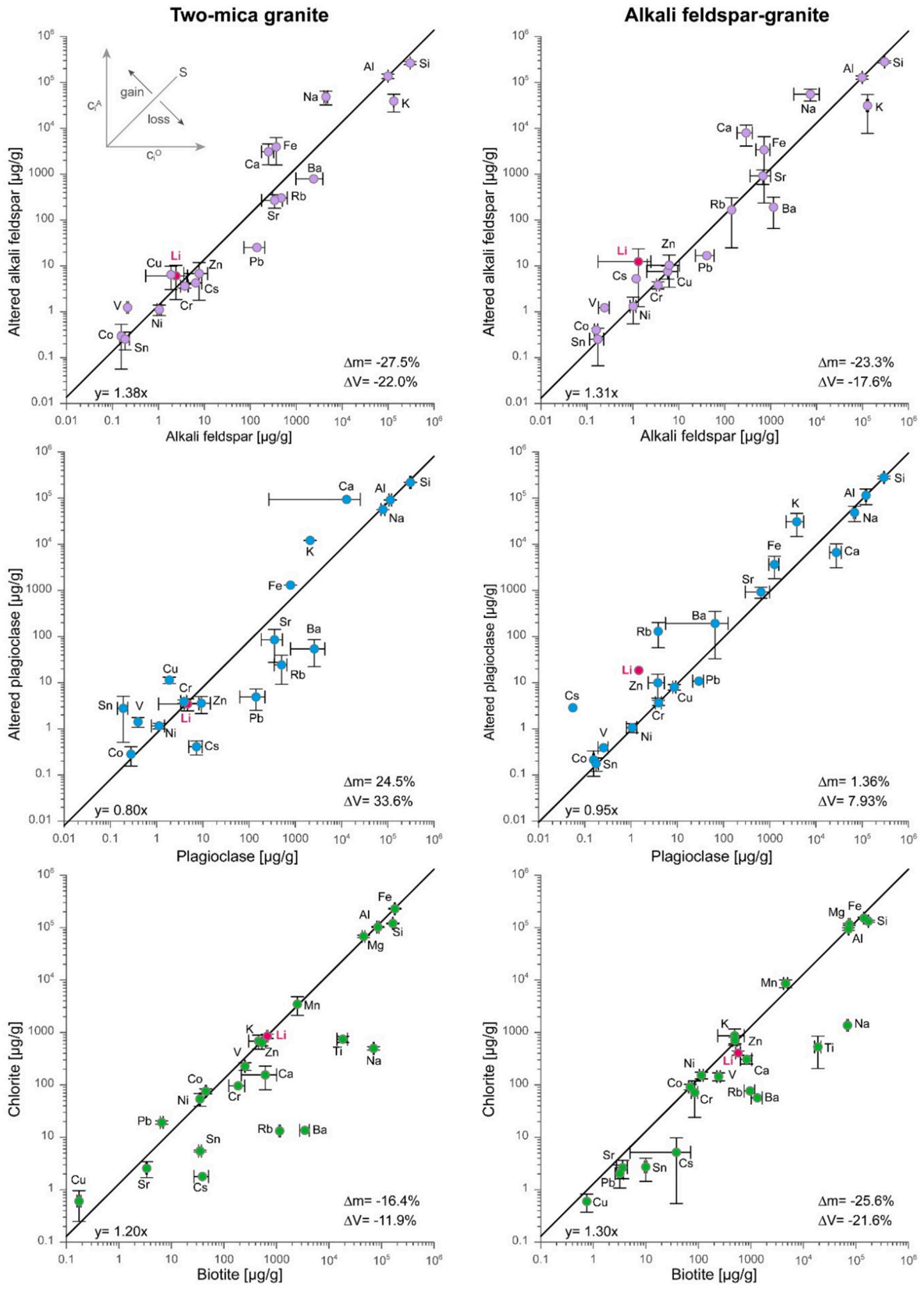

Fig. 13. Isocon diagrams for hydrothermal event 2 and calculated mass (Δm) and volume (ΔV) change including error bars (sometimes smaller than the symbol). Note that Li is enriched in the hydrothermal alteration product during feldspar alteration, and stays immobile or is only released to a minor amount during chloritization. Density data: Biotite: 2.8 g/cm^3 (Fleet, 2003), chlorite: 2.95 g/cm^3 (Deer et al., 2009), alkali feldspar: 2.60 g/cm^3 (Deer et al., 2001), plagioclase: 2.62 g/cm^3 (Deer et al., 2001), sericite: 2.79 g/cm^3 (after Fleet, 2003).

Table 1
Rock volume that needs to be leached by 1 m^3 of fluid in order to reach the Soultz-sous-Forêts brine composition (Sanjuan et al., 2016). Calculation parameters are: mineral content (Chapter 4), mass balance (ES Table 1), rock density (Baillieux et al., 2013) and degree of alteration (10 %). Mean value calculated as the net element flux over all alteration pairs and samples. Negative values indicate element incorporation and represent the rock volume that interacts as a sink for 1 m^3 of the brine. Note that the calculated source and sink rock volumes are reasonable, but strongly differ for the various samples and elements. This indicates a non-uniform source that is likely outside the current Soultz-sous-Forêts reservoir for most of the elements.

		Sou-4	Sou-7	Sou-12	Sou-14	Sou-19	Sou-20	Mean
Si	dm^3	9.87	11.3	11.3	60.9	14.3	7.57	12.1
Fe	dm^3	84.5	176	−487	80.4	867	−72.2	394
Sr	dm^3	−9.71	−6.89	14.8	−20.5	−41.3	14.7	−32.3
Pb	dm^3	32.9	43.6	46.6	171	25.7	6.82	22.5
Ca	m^3	−3.0	−6.1	−4.4	−4.5	13.6	−0.84	−2.89
Na	m^3	−16.9	−17.5	−15.2	81.5	−11.1	−22.6	−19.8
K	m^3	0.34	0.39	0.36	3.63	0.37	0.41	0.44
Mn	m^3	−0.51	−0.59	−1.23	−2.15	−4.28	−3.23	−1.10
Mg	m^3	3.7	−2.5	−0.93	−3.58	−0.83	−0.89	−1.57
Li	m^3	199	36.9	107	364	245	−252	135
Rb	m^3	0.55	12.9	−1.71	−2.32	1.13	0.36	1.32
Cs	m^3	24.4	41.2	−1649	−38.2	−70.1	11.5	54.1
Ba	m^3	0.19	−3.25	0.44	−0.77	0.02	0.01	0.05
Zn	m^3	−0.42	0.58	−1.08	−2.59	−3.14	3.93	−2.93

remain immobile (Fig. 13; cf. Figs. A.1, A.2, Table C.1). Some of the trace elements behave differently during event 2 plagioclase alteration in the two granites, most importantly Li, Ca, Rb and Cs (Fig. 13, Figs. A.1, A.2). The alteration of plagioclase yields variable data for mass and volume gain between 8 and 34 % that reflects the variable element mobility (Fig. 13, Figs. A.1, A.2). During biotite alteration to chlorite most of the elements stay immobile or are depleted (Fig. 13; cf. Figs. A.1, A.2, Table C.1). Typically depleted are Si, Ti, Ca, Na, Ba, Rb, Sr, Cs and Sn. Lithium remains immobile in the two-mica granite, whereas it is slightly depleted in chlorite during biotite alteration in the alkali feldspar-granite (Fig. 13, Figs. A.1, A.2). Biotite alteration to chlorite and titanite yields volume loss between 12 and 22 %, and mass loss between 16 and 26 % (Fig. 13).

Using a bulk density of 2630 kg/m^3 for granite (Baillieux et al., 2013) and a degree of hydrothermal alteration of 10 Vol.-%, which corresponds to our observation of hydrothermally altered samples (Fig. 5), we calculate the rock volume that needs to be leached by 1 m^3 of fluid to reach the composition of the Soultz-sous-Forêts fluid (Chap. 2.3) assuming that the elements were not present in the fluid before interacting with the reservoir rock (Table 1). Negative values indicate element incorporation and represent the rock volume that interacts as a sink for 1 m^3 of the brine. The results are highly variable indicating a non-uniform behaviour of the different solutes, and that the numbers only represent an order of magnitude. Silica is released by most of the hydrothermal alteration reactions and thus, requires only a rock volume of ~20 dm^3 to be leached (Table 1). Potassium needs a rock volume of ~440 dm^3 to be leached, dominantly from K-feldspar decomposition (Table 1). Elevated concentrations of Fe, Ca and Ba in the brine may be explained by leaching of only low volumes of granite, which are still reasonable to equilibrate with only 1 m^3 fluid (Table 1). Interestingly, relatively large maximum volumes of 3.7–81.5 m^3 need to react with the hydrothermal fluid to explain the Na, Mg, Rb and Zn contents (Table 1). Additionally, the granites can act as a sink for most of the elements, especially Sr, Na, Mn, Mg and Zn. In comparison to the other elements, Cs requires larger volumes of ~54 m^3. For Li, a rock volume between approx. 40 and 400 m^3 must react with 1 m^3 fluid (Table 1). The large variability between samples and elements is explained by the different mineralogy and trace element content of the various minerals (Table 1). It shows that local heterogeneity has a large impact on mass balance in fluid-rock interaction.

7. Discussion

In the following, we discuss fluid-rock interaction and quantitative element transfer based on our mass balance data and petrographic observations. We compare our data with quantitative data from hydrothermal experiments (Drüppel et al., 2020; Schmidt et al., 2018) in order to shed light on the source of Li and other trace elements in the Soultz-sous-Forêts geothermal brine. The combination of the analytical data, mass balance calculations and genetic models for the hydrothermal evolution in the Upper Rhine Graben and the Black Forest allows to formulate a new holistic model for complex fluid-rock interaction between granite and connate fluid.

7.1. Element mobility during hydrothermal alteration

Balanced mineral reactions of hydrothermal alteration of the feldspars (Eqs. (4), (5)) are confirmed by mass balance data indicating consumption of Fe and K in plagioclase, while variable behaviour of Ca and Na is explained by different calcite and sericite contents in the alteration assemblage (Figs. 5, 13; Figs. A.1, A.2). Approx. 10 mg/kg SiO_2 is released by K-feldspar alteration and bound in hydrothermal quartz (Fig. 5). Of ~10 mg/kg K released by K-feldspar alteration, ~2 mg/kg K likely is used during sericitization of plagioclase. Approx. 8 mg/kg K are released into the fluid. Calcium is mainly balanced by the formation of calcite, indicating that the hydrothermal fluid had an aqueous-carbonic composition. Trace elements that may be incorporated into sericite (muscovite + illite) and calcite are Li, Rb, Cs, Sr, Ba and Zn. Variable behaviour of these elements is explained by different molar abundance. Consequently, the only trace element consistently and quantitatively released to the fluid by hydrothermal feldspar alteration is Pb. Mass balance indicates that Li, V and locally Rb, Cs, Ba, Cu and Sn tend to be enriched in the mineral assemblage during hydrothermal feldspar alteration, indicating that these elements must be sourced from elsewhere, probably the hydrothermal fluid itself (Figs. A.1, A.2). Differences between our estimation and the one by Dugamin et al. (2024) may be explained by these authors not distinguishing the feldspars.

We observe kaolinite in the proximal event 2 hydrothermal alteration assemblage. Unfortunately, it was impossible to separate distal and proximal assemblages during trace element analysis. It is well-known that kaolinite adsorbs Li (Schroth and Sposito, 1997; Li and Liu, 2020; Chen et al., 2023). Thus, kaolinite may be an additional Li host in the hydrothermal event 2 assemblage. Although the feldspars form the major constituent of the granites, mass balance calculations indicate that hydrothermal alteration of these minerals is not the source of Li in the fluid. Also, elevated Rb, Cs and Sr concentrations in the geothermal brines of Soultz-sous-Forêts are most likely not derived from hydrothermal feldspar alteration alone, although these elements are provided by feldspar alteration in the two-mica granite. It may explain Pb and Ba enrichment in the fluid that subsequently resulted in hydrothermal

galena and baryte in veins and the overlying sandstones (Fig. 10e, f; Walter et al., 2019 and references therein).

Balanced mineral reactions of biotite to chlorite (Eqs. (12), (13)) are supported by mass balance and indicate Si, Ti, Na and Ca loss. These elements are used to form additional event 2 hydrothermal calcite, titanite and quartz. Potassium, Fe, Mg, Mn, Ni and Co remain immobile (Fig. 13). The trace elements Ba, Rb, Cs and Sn are also lost (Fig. 13, Fig. A.2). Lithium is immobile or slightly lost. Thus, the hydrothermal alteration of biotite to chlorite potentially explains the enrichment of Li, Rb, Cs, Sr, Ba and Sn in the geothermal brines of Soultz-sous-Forêts. However, biotite or chlorite comprise only 5–10 Vol-% of the whole rock and rarely all the biotite of a granite sample is completely altered to chlorite. Moreover, the biotite-chlorite reaction in the dominant reservoir rock, the two-mica granite, consumed significant amounts of Pb that must be sourced in the fluid and the feldspars, respectively.

In order to estimate, whether element leaching from the reservoir is a possible process, we calculated the rock volume that needs to react with 1 m^3 fluid to reach the measured fluid composition at Soultz-sous-Forêts (Table 1). It is possible that many of the elements were released to the fluid during hydrothermal alteration, however in particular Li and Cs require unrealistic fluid-rock ratios. Approx. 200 m^3 of granite in the reservoir of Soultz-sous-Forêts needs to equilibrate with 1 m^3 hydrothermal fluid to reach 173 mg Li/L. The results, however, are very variable and thus, must be interpreted carefully (Table 1, Table C.2). The variability is interpreted to reflect different sources for the various elements, e.g. Na and Cs from seawater or evaporite dissolution. Mineral reactions and mass balance data are thus not sufficient alone to make conclusive interpretations on the source of Li and other elements in the geothermal brines of Soultz-sous-Forêts.

7.2. Comparison with hydrothermal alteration experiments

The geochemical and mineralogical effects of hydrothermal alteration of granite in a geothermal reservoir were experimentally determined using the Malsberg Granite, Moldanubian Zone (Schmidt et al., 2018), and granite and monzonite from the Saxothuringian Zone (Drüppel et al., 2020). In the Malsberg Granite, the most important mineral reaction during hydrothermal experiments (1.5 and 2.0 M NaCl solution; 200 and 260 °C) is the alteration of biotite to chlorite along fresh fractures (Schmidt et al., 2018). Notably, biotite alteration to chlorite was also observed in the samples already before the experiments (Schmidt et al., 2018). Feldspars remained largely unaffected, whereas quartz was dissolved. This is different to our observations, where feldspars are locally completely altered to muscovite or illite and kaolinite along fractures (Fig. 9). Silica is produced during the hydrothermal mineral reactions and hydrothermal quartz is formed in altered granite.

The granite and monzonite from the Saxothuringian Zone show various hydrothermal alteration reactions of feldspars to muscovite or illite and kaolinite and also biotite to chlorite or clay minerals, and also dissolution features of quartz (Drüppel et al., 2020). After the

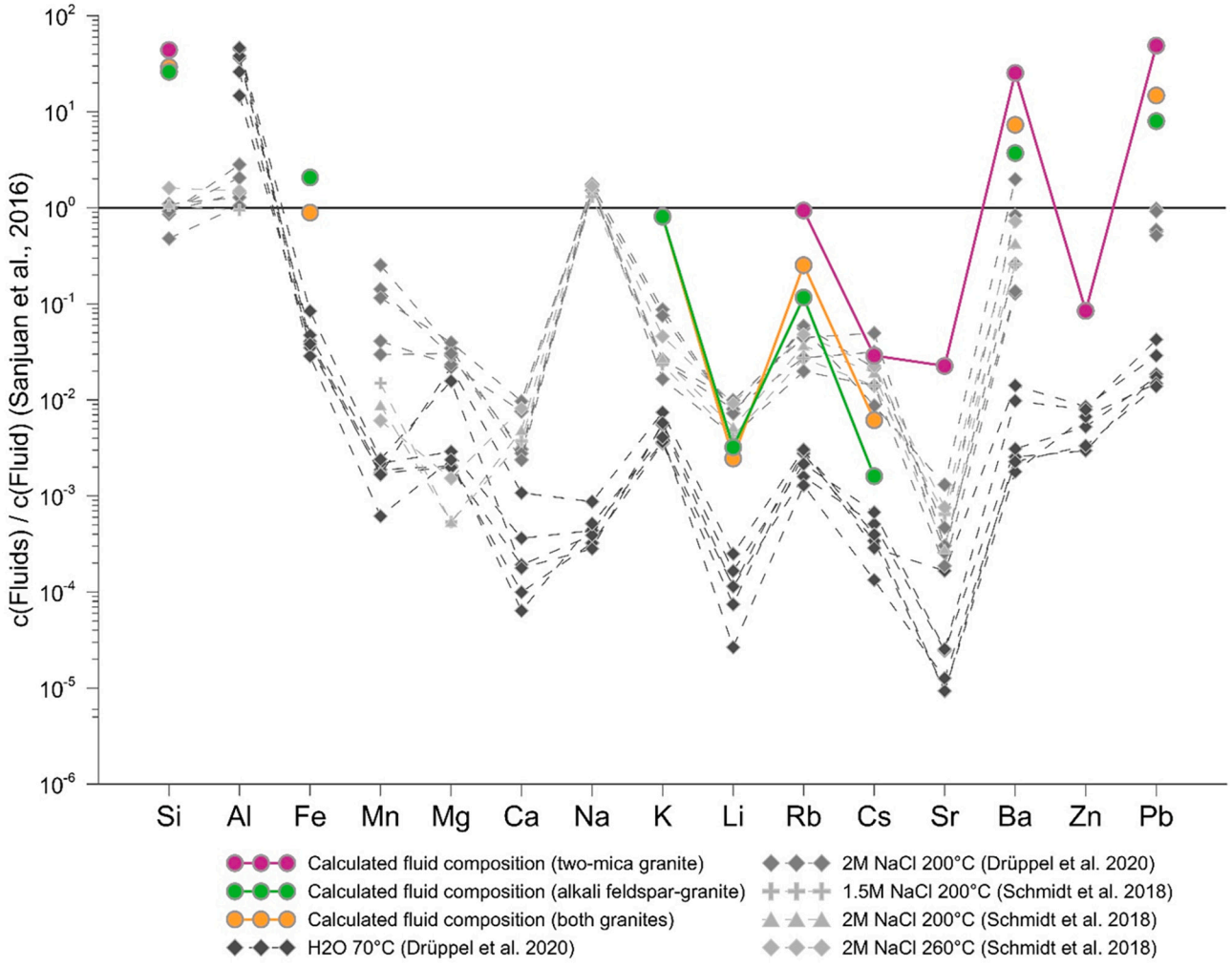

Fig. 14. Composition of the fluids from alteration experiments (Drüppel et al., 2020; Schmidt et al., 2018) and the mass balance calculated fluid composition (this study) in comparison to the geothermal fluid of Soultz-sous-Forêts (Sanjuan et al., 2016).

hydrothermal experiments (2.0 M NaCl solution; 200 °C), the feldspars show albitization and replacement by illite. The biotite is replaced by chlorite and smectite (Drüppel et al., 2020). This is more akin to our observations in granite from Soultz-sous-Forêts, where, however, albitization predates hydrothermal illite alteration and quartz is not dissolved but precipitated from the hydrothermal fluid. This indicates that (1) timing of various hydrothermal alteration events is critical for evaluation of element liberation into a fluid phase; and (2) the simplified brine used in the experiments that only contains Na and Cl may induce hydrothermal alteration that is not representative of natural processes (e.g., quartz dissolution vs. precipitation; Drüppel et al., 2020; Schmidt et al., 2018).

The formation of illite in granitic rocks of the Black Forest that have not been in recent contact with the geothermal brine is dated at 196–142 Ma (Ar-Ar, K-Ar; Bossennec et al., 2021a, 2021b; Brockamp et al., 2003, 2011; Brockamp and Clauer, 2005), which means that hydrothermal event 2 sericite alteration in the reservoir granites of Soultz-sous-Forêts is of similar or younger age. Hydrothermal alteration of biotite to chlorite may be of the same age or even older and related to Variscan syn-magmatic propylitic alteration (Ledésert et al., 1993; Ledésert et al., 1996, 1999, 2010; Gardien et al., 2016; Dubois et al., 1996).

In general, the hydrothermal experiments show that Na, K, Li, Rb, Sr, Ba, Pb and Zn may be leached from the rock samples (Drüppel et al.,

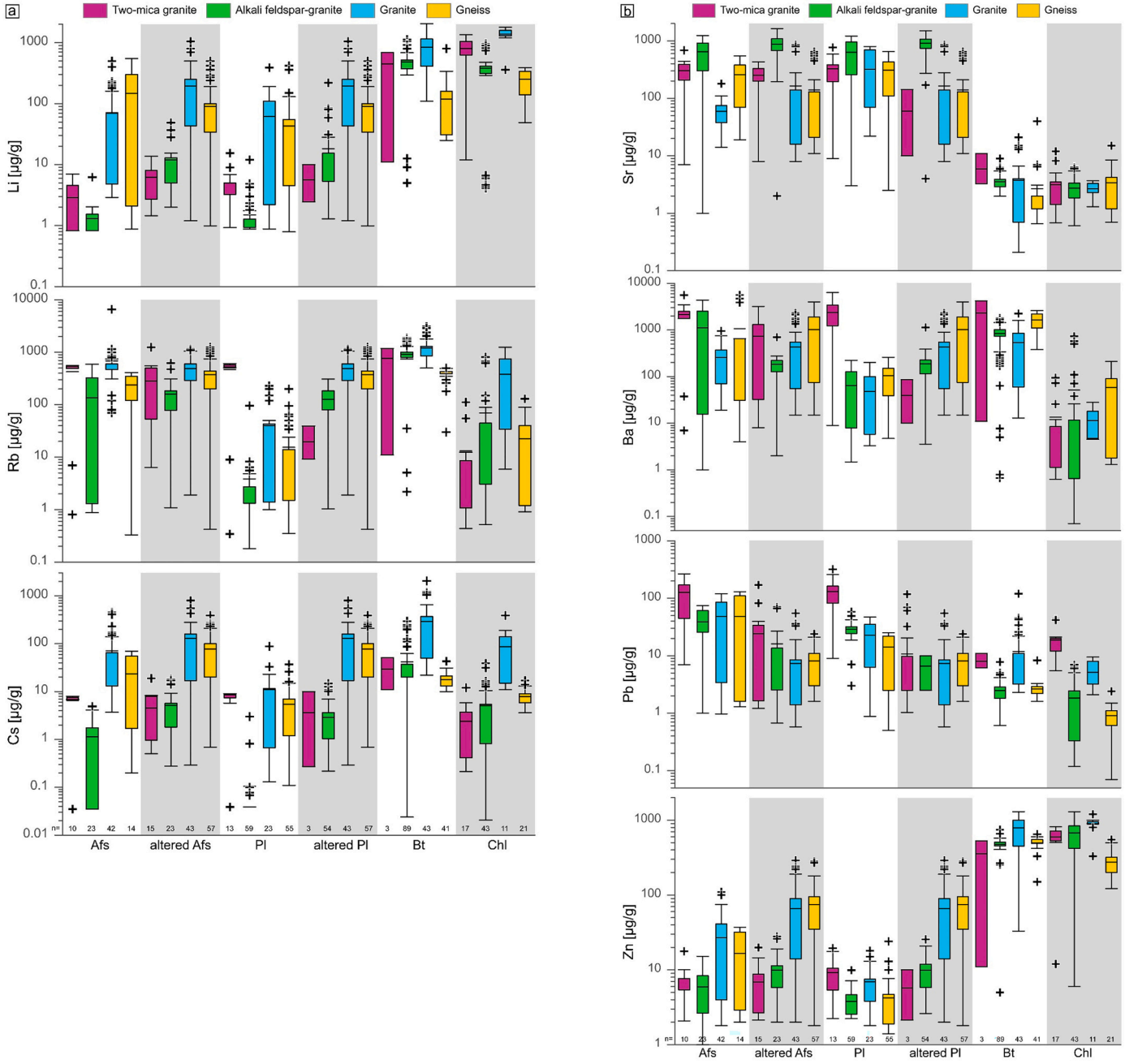

Fig. 15. Boxplot illustrating the trace element distribution for individual minerals sorted after element. Average trace element composition of the samples from the alkali feldspar-granite and two-mica granite of Soultz-sous-Forêts. Trace element concentrations of the granite and gneiss from the Schwarzwald are from Walter et al. (2019) (Table C.3). The order of the rocks corresponds to the order of the legend. a) alkaline elements, b) alkaline earth elements and Pb, Zn. Boxplots represent mean, lower (0.25-quantile) and upper quartile (0.75-quantile), lower and upper whisker and outliers (minimum and maximum values). Data below the detection limit are included with the value of the calculated detection limit (Table B; method of fixed-value imputation adapted from Frenzel (2023)).

2020; Schmidt et al., 2018), which is similar to our observations (Fig. 14). In detail however, the mass balance of feldspar alteration indicates that Li, Cs, Na, Ca and locally Rb are consumed and need already to be present in the fluid in contrast to the hydrothermal experiments that use simplified NaCl solutions (this study; Drüppel et al., 2020). During the experiments, Mn, Mg, Ca, K, Li, Rb, Cs, Sr, Ba, Zn and Pb were not leached to the extent to reach the original fluid composition of Soultz-sous-Forêts (Fig. 14; Drüppel et al., 2020). Our mass balance indicates that many of these elements in fact can reach the level of the original hydrothermal fluid except for Li, Cs, Sr and Zn (Fig. 14). Quartz dissolution in the experiments released trace elements from fluid inclusions that are Li-rich and contain other elements, affecting the experimental leaching data (Drüppel et al., 2020; Walter et al., 2019). In addition, our mass balance calculation indicates that whole rock composition may be critical since the two-mica granite and the alkali feldspar-granite show the same alteration mineral assemblage, but different element behaviour (Fig. 14, Table 1). This means that the hydrothermal experiments using a simplified brine composition only yield a first-order estimate of element mobility.

Experimental leaching of already altered granite samples also provided Na, K, Li, Rb, Sr, Ba, Pb and Zn to the fluid phase (Drüppel et al., 2020; Schmidt et al., 2018). Our mass balance indicates that many of these elements are even enriched during the hydrothermal alteration event 2. This may indicate that elements from feldspars, sericite, biotite and chlorite as well as adsorbed elements on e.g. clay minerals may be released upon further alteration, which would mean that alteration with a diluted brine may cause element leaching and enrichment in the fluid.

7.3. Comparison with the hydrothermal system of the Black Forest

Rocks from the Moldanubian Zone of the Black Forest represent analogues to the granites from Soultz-sous-Forêts and are well investigated in terms of petrology, mineral chemistry and paleo fluid evolution (Altherr et al., 2000; Geyer et al., 2011; Hann et al., 2003; Lardeaux et al., 2014; Skrzypek et al., 2014; Burisch et al., 2016; Walter et al., 2019; Drüppel et al., 2020). First starting with Tertiary rifting, the lithologies in the rift and the rift shoulders underwent a different geological evolution (Walter et al., 2018a, 2018b, 2019). The trace elements in the minerals of the gneiss and granite from the Black Forest and those from Soultz-sous-Forêts granites are in a similar range supporting generally similar petrological evolution (Fig. 15, Table C.3). The rocks of the Black Forest show a greater variability in trace element content of the major minerals (Fig. 15, Table C.3). Biotite and chlorite pairs generally have very similar composition. The same is true for the feldspars and their hydrothermal alteration products, which only have higher Li- and lower Pb-contents in the Black Forest. Since both, petrographic observations and major and trace element data of major minerals in typical rocks of the Moldanubian zone from surface outcrops in the Black Forest and from drill cores transecting the geothermal reservoir at Soultz-sous-Forêts at 2000–5000 m depth are very similar (this study; Drüppel et al., 2020; Dugamin et al., 2024; Walter et al., 2019), the rocks likely underwent a similar hydrothermal evolution of (1) biotite replacement by chlorite during Variscan propylitic alteration (Dubois et al., 1996; Gardien et al., 2016; Ledésert et al., 1993; Ledésert et al., 1996, 1999, 2010) and (2) feldspar replacement by illite between 196 and 142 Ma (Ar-Ar, K-Ar; Bossennec et al., 2021a, 2021b; Brockamp et al., 2003, 2011; Brockamp and Clauer, 2005; Clauer et al., 2008; Meyer et al., 2000; Schleicher et al., 2006; Walter et al., 2016, 2019). The main difference between recent geothermal fluids of Soultz-sous-Forêts and hydrothermal fluids that formed the veins in the Black Forest is that the latter hydrothermal system closed between 40 and 20 Ma (Burisch et al., 2018). Lower Li-contents in the fluids today than in the fluid inclusions may be explained by (1) dilution through mixing with meteoric water or recent connate fluids or (2) depletion of the reservoir rocks by >20–40 Ma hydrothermal alteration and migration of these fluids.

The Li content in minerals of the Black Forest gneiss is, however, generally lower than in the granite (Fig. 15, Table C.3). The feldspars and their hydrothermal alteration products from the Black Forest granite have slightly higher Li (Cs, Rb, Zn) concentrations than in the Soultz-sous-Forêts granites (Fig. 15, Table C.3). This may be explained by leaching of Li from the feldspar, muscovite and illite in the geothermal reservoir rocks of Soultz-sous-Forêts. The hydrothermal experiments equally to mass balance calculations from fluid inclusion data of Mesozoic hydrothermal veins (Walter et al., 2019) also indicate that leaching of Na, K, Li, Rb, Sr, Ba, Pb and Zn from altered granitic rocks from the Black Forest is a feasible process explaining base metal contents in modern and ancient brines (Burisch et al., 2016; Drüppel et al., 2020). However, leaching alone cannot explain the fluid composition at Soultz-sous-Forêts (Fig. 14). The fluid inclusion data of Mesozoic and Cenozoic hydrothermal veins in the Black Forest and Soultz-sous-Forêts show strongly variable but often elevated contents of Na, K, Li, Rb, Sr, Ba, Pb and Zn compared to the modern brine (up to 5 wt.-% Li; Dugamin et al., 2024; Walter et al., 2018a, 2019, 2020a). Since the Mesozoic brines analysed in the hydrothermal veins are mixed fluids and in disequilibrium with the country rocks, the direct comparison with geothermal fluids from Soultz-sous-Forêts may not be applicable, since the latter are considered at least partly in chemical equilibrium with the reservoir rocks (Sanjuan et al., 2010, 2016, 2022). It may, however, indicate that the recent fluids evolved from such Mesozoic brines.

7.4. Genetic model of hydrothermal alteration and element transfer in reservoir rocks from Soultz-sous-Forêts

The balanced mineral reactions in conjunction with mass balance calculations indicate that hydrothermal alteration of feldspar to sericite significantly released Si, Na, K and Pb to a hydrothermal fluid, whereas hydrothermal alteration of biotite to chlorite released Si, Ti, Fe, Na, K and all analysed trace elements (Fig. 13). This is consistent with experimental data of granite leaching (Drüppel et al., 2020; Schmidt et al., 2018) and petrographic, geochemical and fluid inclusion data (Dugamin et al., 2024), assuming that all hydrothermal alteration reactions are coeval. Our mass balance data confirms this for Si, Fe, Ca, K, Rb, Sr, Zn and Pb, which may be leached at relevant concentrations from a relatively low volume of granite (Table 1). The hydrothermal alteration minerals quartz, calcite and titanite used some of the elements provided by feldspar and biotite alteration. Manganese, Mg, Na, Li, Cs, Ba and likely Cl contents of the geothermal fluid at Soultz-sous-Forêts cannot solely and easily be explained by leaching of the granite reservoir rock. Most of these elements are released by the alteration of biotite to chlorite, except for Ca and Na which are provided by plagioclase alteration. In particular, Li is only released significantly through chloritization of biotite, and further alteration to illite (Dugamin et al., 2024). Given the low amount of biotite and chlorite present in the reservoir rock, our balanced mineral reactions and mass balance calculations show that during hydrothermal alteration of biotite to chlorite not enough Li is released to explain the observed Li-content in the geothermal fluid at Soultz-sous-Forêts. In the case of Li, this fact was previously discussed for geochemical fluid data and hydrothermal experiments (Drüppel et al., 2020; Sanjuan et al., 2016), although geochemical calculations using whole rock data indicate that only 10 % of granite must be leached to reach the current Li content at Soultz-sous-Forêts (Dugamin et al., 2024). This data, however, does not consider the detailed mass balance of the hydrothermal alteration reactions of our study.

The early stages of hydrothermal alteration of the granitic rocks from surface outcrops in the Black Forest and from Soultz-sous-Forêts drill cores are similar and thus, can be compared to the hydrothermal systems extensively investigated in the Black Forest. Unfortunately, no data is available for Variscan propylitic alteration of the granite and similar mineral-fluid reactions may have occurred subsequently. This early hydrothermal stage is overprinted by two major events (Fig. 16):

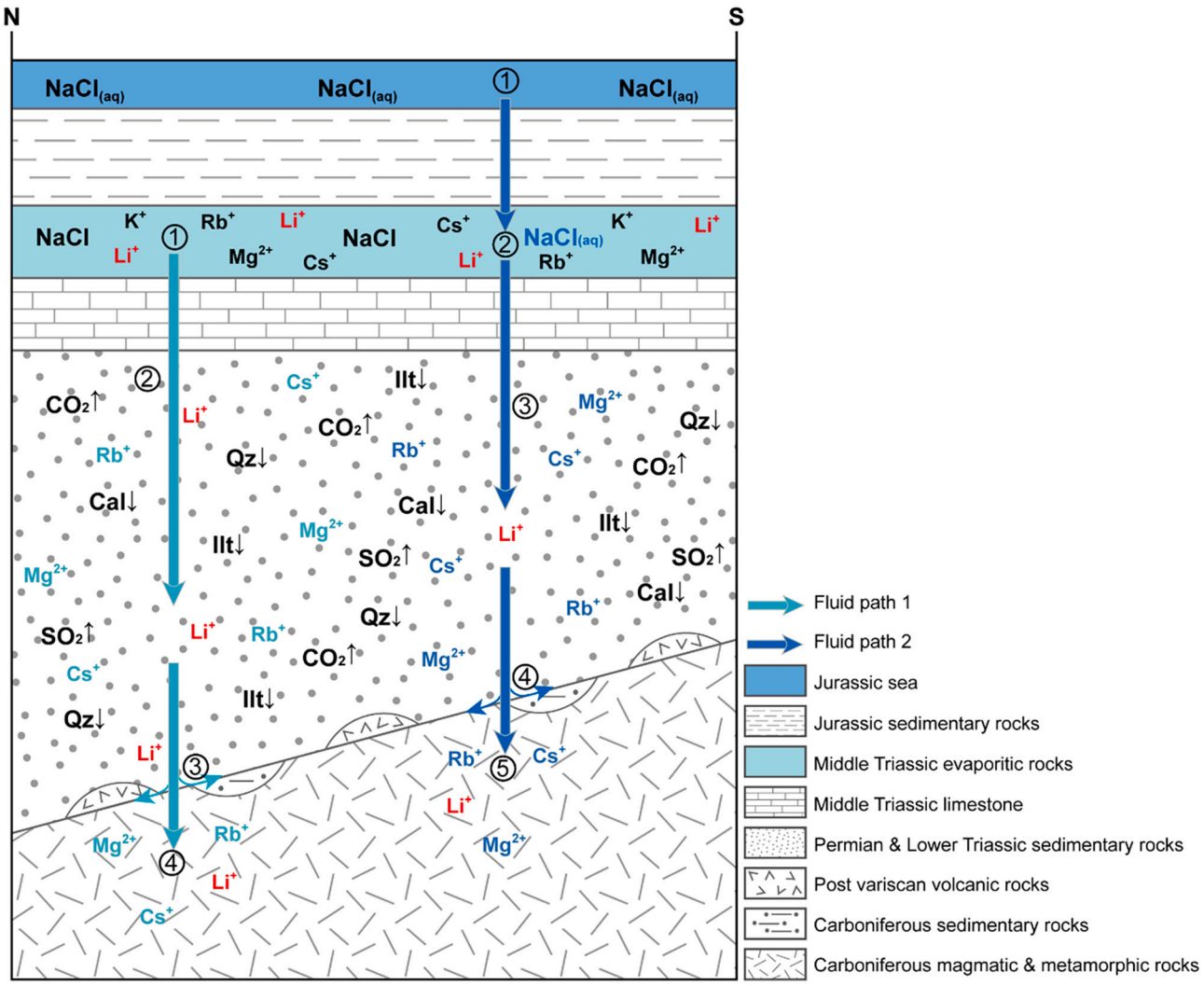

Fig. 16. Simplified hydrothermal evolution model for Soultz-sous-Forêts. Scenario 1: Fluid 1 is a Middle Triassic bittern brine with high salinity and T = 120–150 °C (Boiron et al., 2010; Cathelineau and Boiron, 2010; Dugamin et al., 2024); 1) stratification and infiltration in Middle Triassic limestone; 2) infiltration in Permian and Lower Triassic sedimentary rocks, precipitation of calcite, illite, quartz, degassing of CO_2 and SO_2; 3) infiltration of the fluid in the Variscan basement and circulation along the unconformity between Permian and Triassic-formations and the Variscan basement. Scenario 2: Fluid 2 is Jurassic seawater; 1) infiltration in the subsurface 2) infiltration and dissolution of Middle Triassic evaporite and limestone, mixing with Fluid 1; 3) infiltration in Permian and Lower Triassic sedimentary rocks, precipitation of calcite, illite, quartz, degassing of CO_2 and SO_2; 3) infiltration of the hot (T = 150–190 °C) low salinity fluid (Boiron et al., 2010; Cathelineau and Boiron, 2010; Dugamin et al., 2024) in the Variscan basement and circulation along the unconformity between Permian and Triassic-formations and the Variscan basement.

(1) During the Middle Triassic, bittern brines (Na-Ca-Cl-CO_3-SO_4 fluids) enriched in Li, Rb, and Cs migrated downwards due to their higher density into granite and gneiss of the Moldanubian Zone (Boiron et al., 2010; Cathelineau and Boiron, 2010; Bons et al., 2014). This resulted in fluid-rock interaction and hydrothermal alteration, modifying the bittern brine and the wall rocks at 120–150 °C (Boiron et al., 2010; Cathelineau and Boiron, 2010; Dugamin et al., 2024; Walter et al., 2016). Hydration of the wall rocks consumed water and residually enriched the brine salinity (Burisch et al., 2016; Walter et al., 2019). This hydrothermal alteration event may be related to the albitization of the feldspars, initial sericite alteration, and possibly the reaction of biotite to chlorite. This is supported by our data that indicates addition of Na, K, Ca, Li, Cs and Rb from a hydrothermal fluid during feldspar alteration (Figs. 5, 7, Table B). In addition, the Li-rich chlorite may also have formed by interaction with such a Li-rich brine.

(2) From the Jurassic until the Cenozoic, lower salinity marine water penetrated the subsurface and dissolved Middle Muschelkalk anhydrite, gypsum and halite formations and locally the Oligocene halite- and bitter salt-bearing Pechelbronn Formation (Fig. 1). The resulting halite-dissolution brine is Na-dominated and descends through the Lower Triassic and Lower Permian sandstone into the crystalline rocks triggered by higher density and ongoing desiccation by hydration of the crystalline rocks at 150–190 °C (Fig. 1; Bons et al., 2014; Scharrer et al., 2022). This fluid mixed with the slightly colder, modified bittern brine forming widespread fluorite-baryte veins (Boiron et al., 2010; Cathelineau and Boiron, 2010; Dugamin et al., 2024; Walter et al., 2016, 2017, 2018a, 2018b, 2019). The fluid inclusions in such hydrothermal veins show Li-contents of up to 5 wt.-% (Dugamin et al., 2024; Walter et al., 2016, 2017, 2018a, 2018b, 2019), which proves significant Li-transport in Jurassic-Cretaceous times (Staude et al., 2009; Burisch et al., 2016; Walter et al., 2019). The hydrothermal illite produced during feldspar alteration is dated exactly at this time (Bossennec et al., 2021a, 2021b; Brockamp et al., 2003, 2011; Brockamp and Clauer, 2005; Clauer et al., 2008; Meyer et al., 2000; Schleicher et al., 2006;

Walter et al., 2016, 2019), supporting this scenario. This would however mean, that the geothermal brine at Soultz-sous-Forêts is the result of a complex, ~150 m.y. hydrothermal evolution.

This complex evolution is in contrast to the interpretation based on salinity, Cl-Br ratio and traditional stable isotopes that the geothermal brines formed by mixing of Mesozoic and/or Cenozoic evaporated marine fluid with meteoric fluid and subsequent fluid-rock interaction at 225 °C in the sandstone of the Lower Triassic Buntsandstein (Sanjuan et al., 2016, 2022). Although Cl/Br and Rb/Cs ratios as well as traditional stable isotope data indicate long-term water-rock interaction between the geothermal fluid and the reservoir rocks, Li, B, Sr and Nd isotopes cannot be explained by fluid-rock interaction with granite alone (Sanjuan et al., 2010, 2016). These isotope systems rather yield mixed results or indicate interaction with the white mica and biotite of the mica-rich sandstone of the Buntsandstein, where the Li-source is interpreted to be situated (Dugamin et al., 2024; Kölbel et al., 2023; Sanjuan et al., 2010, 2016, 2022). However, whole-rock geochemical data show still high Li-contents (20–80 mg/kg) at Bruchsal, Germany (Kölbel et al., 2023), rather indicating that these rocks have not been leached and depleted in Li and may not represent a likely source. This is thus, in favour of the model (1) presented above, where Jurassic-Cretaceous fluids interacted with sedimentary rocks during migration (Fig. 16). This would mean that the fluids are not derived from the rift shoulder (Stober and Bucher, 2015a), because the hydrothermal evolution started earlier than rifting of the Upper Rhine Graben.

Our petrographic and mass balance data indicate that Na, Li, Cs, Cl and CO_2 must be sourced outside the geothermal reservoir and brought to the granitic host rocks via the migration of connate fluids. The Li-content correlates with Na- and Cl-contents (Drüppel et al., 2020; Dugamin et al., 2024; Sanjuan et al., 2010, 2016, 2022). This, in conjunction with the genetic model for hydrothermal vein systems in the Black Forest, indicates that the critical parameters for the development of a Li resource are fluid mixing of older connate water with younger connate waters that interacted with the sedimentary strata during descent. The correlation of Li with Na and Cl, the evidence of halite dissolution and interaction with carbonated sediments indicates that interaction with red bed sediments, evaporites and their residual brines is critical. Such a process also explains the enrichment of Cs, Cl, CO_2 and other elements that are involved in the hydrothermal processes. Lithium-rich brines in the Upper Rhine Graben are mainly known from aquifers in Variscan crystalline rocks of the Moldanubian Zone (Soultz-sous-Forêts) and the Mid German Crystalline High (Insheim, Landau) and Permo-Triassic sedimentary rocks (Bruchsal). The second critical parameter of the Li-mineral system is preservation, which means that the reservoirs are not connected to the surface and brine is discharged into other aquifers or to the surface in thermal springs (Fig. 1b).

8. Conclusion

We distinguish two main hydrothermal alteration events in granitic reservoir rocks from Soultz-sous-Forêts that are similar to equivalent lithologies from the Black Forest:

1. K-feldspar and plagioclase have albite rims and patchy albite zones
2. Feldspars are replaced by sericite and calcite, and kaolinite in proximal alteration zones, biotite is replaced by chlorite and locally titanite

Mineral reactions of the hydrothermal alteration stage 2 release Si, K, Na and Ti, which are incorporated into the alteration minerals and additional hydrothermal quartz, calcite and titanite. In order to balance for mass, Na, Ca, Li, Cs, Ba and Cl are required from the hydrothermal fluid, indicating an additional external source. The Li and other elements content in the geothermal fluid may thus be explained by the complex evolution of connate fluids in the Upper Rhine Graben, with intense fluid-rock interaction and an additional source in evaporites of Oligocene or Middle Triassic age. Critical parameters are:

1. Middle Triassic bittern brines (Na-Ca-Cl-CO_3-SO_4 fluids, high salinity, T = 120–150 °C) enriched in Li, Rb, and Cs that migrated into the reservoir rocks and caused hydrothermal alteration event 1.
2. Jurassic-Cretaceous marine water (low salinity, T = 150–190 °C) that dissolved evaporites and was subsequently enriched in Na, Li, Cs, Cl and CO_2 that mixed with the bittern brine in the reservoir and resulted in hydrothermal alteration event 2.
3. Sufficient porosity in the reservoir that allows a large geothermal water resource to be stored but additionally disconnection to the surface or other aquifers to avoid mixing and dilution.

Although we can show that hydrothermal alteration and related element mobility are strongly dependent on the rock type even in detail (alkali feldspar-granite vs. two-mica granite), fluid-rock interaction in the granitic reservoir must not be considered as the exclusive process of Li-resource development. The Li-enriched nature of the hydrothermal alteration assemblage may represent an additional Li resource upon mining when the Li-content in the brine is reduced significantly and no new minerals are formed that incorporate or adsorb the Li.

CRediT authorship contribution statement

Michèle Jungmann: Writing – original draft, Visualization, Validation, Methodology, Investigation, Formal analysis, Data curation, Conceptualization. **Benjamin F. Walter:** Writing – review & editing, Writing – original draft, Supervision, Funding acquisition. **Elisabeth Eiche:** Writing – review & editing, Resources, Funding acquisition. **R. Johannes Giebel:** Methodology, Data curation. **Jochen Kolb:** Writing – review & editing, Writing – original draft, Supervision, Resources, Project administration, Funding acquisition, Conceptualization.

Declaration of competing interest

The authors declare the following financial interests/personal relationships which may be considered as potential competing interests: Jungmann reports financial support, administrative support, and travel were provided by German Research Foundation. If there are other authors, they declare that they have no known competing financial interests or personal relationships that could have appeared to influence the work reported in this paper.

Data availability

Data will be made available on request.

Acknowledgements

Rebekka Reich is thanked for helpful discussions concerning mineral analysis and chemistry, and Dominik Gudelius for his help during LA-ICPMS analysis. We thank Albert Genter from ÉS-Géothermie for providing the drill core samples from the GEIE EMC of Soultz-sous-Forêts. Furthermore, we acknowledge Thomas Wenzel, Sebastian Staude, and Thomas Binder of the University of Tübingen for their support on the microprobe. We would like to thank the German Research Foundation (DFG) for financial support for the acquisition of the electron microprobe (grant: INST 37/1026-1 FUGG) at the University of Tübingen and for the acquisition of the LA-ICP-MS (INST 121384/213-1 FUGG) at KIT. We would like to thank the Editor Stefano Albanese as well as the anonymous reviewers for their comments and revisions that significantly improved the quality of this article. This research is part of the project Energy and Mass fluxes in the Upper Rhine Graben (EMURG) funded by the German Research Foundation (DFG), grant no. KO 2072/4-1.

Appendix A. Supplementary data

Supplementary data to this article can be found online at https://doi.org/10.1016/j.gexplo.2024.107641.

References

Agemar, T., Schellschmidt, R., Schulz, R., 2012. Subsurface temperature distribution in Germany. Geothermics 44, 65–77. https://doi.org/10.1016/j.geothermics.2012.07.002.

Agemar, T., Brunken, J., Jodocy, M., Schellschmidt, R., Schulz, R., Stober, I., 2013. Untergrundtemperaturen in Baden-Württemberg. Z. Dtsch. Ges. Geowiss. 164, 49–62. https://doi.org/10.1127/1860-1804/2013/0010.

Agemar, T., Alten, J.-A., Ganz, B., Kuder, J., Kühne, K., Schumacher, S., Schulz, R., 2014. The Geothermal Information System for Germany – GeotIS. Z. Dtsch. Ges. Geowiss. 165, 129–144. https://doi.org/10.1127/1860-1804/2014/0060.

Aichholzer, C., Duringer, P., Orciani, S., Genter, A., 2016. New stratigraphic interpretation of the Soultz-sous-Forêts 30-year-old geothermal wells calibrated on the recent one from Rittershoffen (Upper Rhine Graben, France). Geotherm. Energy 4. https://doi.org/10.1186/s40517-016-0055-7.

Aichholzer, C., Duringer, P., Genter, A., 2019. Detailed descriptions of the lower-middle Triassic and Permian formations using cores and gamma-rays from the EPS-1 exploration geothermal borehole (Soultz-sous-Forêts, Upper Rhine Graben, France). Geotherm. Energy 7. https://doi.org/10.1186/s40517-019-0148-1.

Alexandrov, P., Royer, J.-J., Deloule, É., 2001. 331 ± 9 Ma emplacement age of the Soultz monzogranite (Rhine Graben basement) by U/Pb ion-probe zircon dating of samples from 5 km depth. C. R. Acad. Sci. Ser. IIA Earth Planet. Sci. 332, 747–754. https://doi.org/10.1016/S1251-8050(01)01594-4.

Altherr, R., Holl, A., Hegner, E., Langer, C., Kreuzer, H., 2000. High-potassium, calc-alkaline I-type plutonism in the European Variscides: northern Vosges (France) and northern Schwarzwald (Germany). Lithos 50, 51–73. https://doi.org/10.1016/S0024-4937(99)00052-3.

Anders, B., Beccaletto, L., Capar, L., Mermy, D.C., Dezayes, C., Dresmann, H., Elsass, P., Fehn, C., Fischer, G., Franz, M., Haneke, J., Huggenberger, P., Kärcher, T., Krzyzanowski, J., Nitsch, E., Oliviero, G., Prestel, R., Rodat, C., Rupf, I., Schuff, J., Siemon, S., Sokol, G., Storz, R., Tesch, J., Urban, S., Weidenfeller, M., Wielandt-Schuster, U., Wirsing, G., Zumsprekel, H., 2013a. Geopotenziale des tieferen Untergrundes im Oberrheingraben: Fachlich-Technischer Abschlussbericht des INTERREG-Projekts GeORG, Teil 2: Geologische Ergebnisse und Nutzungsmöglichkeiten. LGRB-Informationen 28, Freiburg i. Br./Mainz/Strasbourg/Basel.

Anders, B., Beccaletto, L., Capar, L., Mermy, D.C., Dezayes, C., Dresmann, H., Elsass, P., Fehn, C., Fischer, G., Franz, M., Haneke, J., Huggenberger, P., Kärcher, T., Krzyzanowski, J., Nitsch, E., Oliviero, G., Prestel, R., Rodat, C., Rupf, I., Schuff, J., Siemon, S., Sokol, G., Storz, R., Tesch, J., Urban, S., Weidenfeller, M., Wielandt-Schuster, U., Wirsing, G., Zumsprekel, H., 2013b. Geopotenziale des tieferen Untergrundes im Oberrheingraben: Fachlich-Technischer Abschlussbericht des INTERREG-Projekts GeORG, Teil 4: Atlas. LGRB-Informationen 28, Freiburg i. Br./Mainz/Strasbourg/Basel.

Aquilina, L., Pauwels, H., Genter, A., Fouillac, C., 1997. Water-rock interaction processes in the Triassic sandstone and the granitic basement of the Rhine Graben: geochemical investigation of a geothermal reservoir. Geochim. Cosmochim. Acta 61, 4281–4295. https://doi.org/10.1016/S0016-7037(97)00243-3.

Aretz, A., Bär, K., Götz, A.E., Sass, I., 2016. Outcrop analogue study of Permocarboniferous geothermal sandstone reservoir formations (northern Upper Rhine Graben, Germany): impact of mineral content, depositional environment and diagenesis on petrophysical properties. Geol. Rundsch. 105, 1431–1452. https://doi.org/10.1007/s00531-015-1263-2.

Armstrong, J.T., 1991. Quantitative elemental analysis of individual microparticles with electron beam instruments. In: Heinrich, K.F.J. (Ed.), Electron Probe Quantitation, 1st ed. Springer, New York, NY, pp. 261–315.

Baatartsogt, B., Schwinn, G., Wagner, T., Taubald, H., Beitter, T., Markl, G., 2007. Contrasting paleofluid systems in the continental basement: a fluid inclusion and stable isotope study of hydrothermal vein mineralization, Schwarzwald district, Germany. Geofluids 7, 123–147. https://doi.org/10.1111/j.1468-8123.2007.00169.x.

Baillieux, P., Schill, E., Edel, J.-B., Mauri, G., 2013. Localization of temperature anomalies in the Upper Rhine Graben: insights from geophysics and neotectonic activity. Int. Geol. Rev. 55, 1744–1762. https://doi.org/10.1080/00206814.2013.794914.

Bartier, D., Ledésert, B., Clauer, N., Meunier, A., Liewig, N., Morvan, G., Addad, A., 2008. Hydrothermal alteration of the Soultz-sous-Forêts granite (Hot Fractured Rock geothermal exchanger) into a tosudite and illite assemblage. Eur. J. Mineral. 20, 131–142. https://doi.org/10.1127/0935-1221/2008/0020-1787.

Becker, R., Reischmann, T. (Eds.), 2021. Geologie von Hessen. Schweizerbart, Stuttgart (705 pp.).

Binder, T., Marks, M.A.W., Gerdes, A., Walter, B.F., Grimmer, J., Beranoguirre, A., Wenzel, T., Markl, G., 2022. Two distinct age groups of melilitites, foidites, and basanites from the southern Central European Volcanic Province reflect lithospheric heterogeneity. Int. J. Earth Sci. https://doi.org/10.1007/s00531-022-02278-y.

Bjørkum, P.A., Gjelsvik, N., 1988. An isochemical model for formation of authigenic kaolinite, K-feldspar and illite in sediments. J. Sediment. Res. 58. https://doi.org/10.1306/212F8DD2-2B24-11D7-8648000102C1865D.

BMWK, 2022. Informationsportal Erneuerbare Energien. Bundesministerium für Wirtschaft und Klimaschutz. https://www.erneuerbare-energien.de/EE/Navigation/DE/Home/home.html. (Accessed 28 February 2023).

Boiron, M.-C., Cathelineau, M., Richard, A., 2010. Fluid flows and metal deposition near basement/cover unconformity: lessons and analogies from Pb-Zn-F-Ba systems for the understanding of Proterozoic U deposits. Geofluids. https://doi.org/10.1111/j.1468-8123.2010.00289.x.

Bons, P.D., Fusswinkel, T., Gomez-Rivas, E., Markl, G., Wagner, T., Walter, B.F., 2014. Fluid mixing from below in unconformity-related hydrothermal ore deposits. Geology 42, 1035–1038. https://doi.org/10.1130/G35708.1.

Bossennec, C., Géraud, Y., Böcker, J., Klug, B., Mattioni, L., Bertrand, L., Moretti, I., 2021a. Characterisation of fluid flow conditions and paths in the Buntsandstein Gp. sandstones reservoirs, Upper Rhine Graben. BSGF - Earth Sciences. Bulletin 192, 35. https://doi.org/10.1051/bsgf/2021027.

Bossennec, C., Géraud, Y., Böcker, J., Klug, B., Mattioni, L., Sizun, J.-P., Sudo, M., Moretti, I., 2021b. Evolution of diagenetic conditions and burial history in Buntsandstein Gp. fractured sandstones (Upper Rhine Graben) from in-situ δ18O of quartz and 40Ar/39Ar geochronology of K-feldspar overgrowths. Int. J. Earth Sci. 1–24. https://doi.org/10.1007/s00531-021-02080-2.

Boy, J., Steingötter, K. (Eds.), 2005. Geologie von Rheinland-Pfalz: Mit 36 Tabellen im Text. Schweizerbart, Stuttgart (400 pp.).

Brockamp, O., Clauer, N., 2005. A km-scale illite alteration zone in sedimentary wall rocks adjacent to a hydrothermal fluorite vein deposit. Clay Miner. 40, 245–260. https://doi.org/10.1180/0009855054020170.

Brockamp, O., Clauer, N., Zuther, M., 2003. Authigenic sericite record of a fossil geothermal system: the Offenburg trough, central Black Forest, Germany. Int. J. Earth Sci. 92, 843–851. https://doi.org/10.1007/s00531-003-0368-1.

Brockamp, O., Schlegel, A., Clauer, N., 2011. Mesozoic hydrothermal impact on Rotliegende and Bunter immature sandstones of the High Rhine trough and its adjacent eastern area (southern Black Forest, Germany). Sediment. Geol. 234, 76–88. https://doi.org/10.1016/j.sedgeo.2010.12.001.

Bundesverband Geothermie e.V., 2023. Tiefe Geothermieprojekte in Deutschland. https://www.geothermie.de/fileadmin/user_upload/Aktuelles/Projektliste_Tiefe_Geothermie_2023_intern_Stand_Februar_20230228.pdf. (Accessed 5 April 2023).

Burisch, M., Marks, M.A.W., Nowak, M., Markl, G., 2016. The effect of temperature and cataclastic deformation on the composition of upper crustal fluids — an experimental approach. Chem. Geol. 433, 24–35. https://doi.org/10.1016/j.chemgeo.2016.03.031.

Burisch, M., Walter, B.F., Gerdes, A., Lanz, M., Markl, G., 2018. Late-stage anhydrite-gypsum-siderite-dolomite-calcite assemblages record the transition from a deep to a shallow hydrothermal system in the Schwarzwald mining district, SW Germany. Geochim. Cosmochim. Acta 223, 259–278. https://doi.org/10.1016/j.gca.2017.12.002.

Cathelineau, M., Boiron, M.-C., 2010. Downward penetration and mixing of sedimentary brines and dilute hot waters at 5km depth in the granite basement at Soultz-sous-Forêts (Rhine graben, France). Compt. Rendus Geosci. 342, 560–565. https://doi.org/10.1016/j.crte.2009.08.010.

Chen, Y., Zhao, H., Xia, M., Cheng, H., 2023. Insights into lithium adsorption by coal-bearing strata kaolinite. Front. Earth Sci. 17, 251–261. https://doi.org/10.1007/s11707-022-0989-y.

Clauer, N., Liewig, N., Ledesert, B., Zwingmann, H., 2008. Thermal history of Triassic sandstones from the Vosges Mountains-Rhine Graben rifting area, NE France, based on K-Ar illite dating. Clay Miner. 43, 363–379. https://doi.org/10.1180/claymin.2008.043.3.03.

Coffey, D.M., Munk, L.A., Ibarra, D.E., Butler, K.L., Boutt, D.F., Jenckes, J., 2021. Lithium storage and release from lacustrine sediments: implications for lithium enrichment and sustainability in continental brines. Geochem. Geophys. Geosyst. 22. https://doi.org/10.1029/2021GC009916.

Deer, W.A., Howie, R.A., Zussman, J., 2001. Framework Silicates: Feldspars, 2nd ed. Geological Society, London. (972 pp.).

Deer, W.A., Howie, R.A., Zussman, J., 2009. Layered Silicates Excluding Micas and Clay Minerals, 2nd ed. Geological Soc, London. (314 pp.).

Dezayes, C., Chèvremont, P., Tourlière, B., Homeier, G., Genter, A., 2005a. Geological Study of the GPK4 HFR Borehole and Correlation With the GPK3 Borehole (Soultz-Sous-Forêts, France): Final Report BRGM/RP-53697-FR. Bureau de recherches géologiques et minières.

Dezayes, C., Gentier, S., Genter, A., 2005b. Deep Geothermal Energy in Western Europe: The Soultz Project RP-54227-FR. BRGM.

Drüppel, K., Stober, I., Grimmer, J.C., Mertz-Kraus, R., 2020. Experimental alteration of granitic rocks: Implications for the evolution of geothermal brines in the Upper Rhine Graben, Germany. Geothermics 88, 101903. https://doi.org/10.1016/j.geothermics.2020.101903.

Dubois, M., Ayt Ougougdal, M., Meere, P., Royer, J.-J., Boiron, M.-C., Cathelineau, M., 1996. Temperature of paleo- to modern self-sealing within a continental rift basin: the fluid inclusion data (Soultz-sous-Forêts, Rhine graben, France). Eur. J. Mineral. 8, 1065–1080. https://doi.org/10.1127/ejm/8/5/1065.

Dugamin, E.J.M., Cathelineau, M., Boiron, M.-C., Richard, A., Despinois, F., 2023. Lithium enrichment processes in sedimentary formation waters. Chem. Geol. 635, 121626. https://doi.org/10.1016/j.chemgeo.2023.121626.

Dugamin, E.J.M., Boiron, M.-C., Cathelineau, M., Richard, A., Peiffert, C., Lebreton, A., Banks, D.A., Despinois, F., 2024. Brine-granite interaction and lithium leaching in a continental rift (Soultz-sous-Forêts, Rhine Graben, France). Lithos 478-479, 107604. https://doi.org/10.1016/j.lithos.2024.107604.

Epp, T., Walter, B.F., Scharrer, M., Lehmann, G., Henze, K., Heimgärtner, C., Bach, W., Markl, G., 2019. Quartz veins with associated Sb-Pb-Ag±Au mineralization in the Schwarzwald, SW Germany: a record of metamorphic cooling, tectonic rifting, and

element remobilization processes in the Variscan belt. Mineral. Deposita 54, 281–306. https://doi.org/10.1007/s00126-018-0855-8.
Fleet, M.E., 2003. Sheet Silicates: Micas, 2nd ed. Geological Society, London. (758 pp.).
Fontes, J.C., Matray, J.M., 1993. Geochemistry and origin of formation brines from the Paris Basin, France: 1. Brines associated with Triassic salts. Chem. Geol. 109, 149–175. https://doi.org/10.1016/0009-2541(93)90068-T.
Frenzel, M., 2023. Making sense of mineral trace-element data – how to avoid common pitfalls in statistical analysis and interpretation. Ore Geol. Rev. 159, 105566. https://doi.org/10.1016/j.oregeorev.2023.105566.
Frey, M., Bär, K., Stober, I., Reinecker, J., van der Vaart, J., Sass, I., 2022. Assessment of deep geothermal research and development in the Upper Rhine Graben. Geotherm. Energy 10. https://doi.org/10.1186/s40517-022-00226-2.
Fridleifsson, I.B., 2001. Geothermal energy for the benefit of the people. Renew. Sust. Energ. Rev. 5, 299–312. https://doi.org/10.1016/S1364-0321(01)00002-8.
Gardien, V., Rabinowicz, M., Vigneresse, J.-L., Dubois, M., Boulvais, P., Martini, R., 2016. Long-lived interaction between hydrothermal and magmatic fluids in the Soultz-sous-Forêts granitic system (Rhine Graben, France). Lithos 246–247, 110–127. https://doi.org/10.1016/j.lithos.2015.12.002.
GEMOC ARC National Key Centre, 2022. GLITTER. ARC National Key Centre for Geochemical Evolution and Metallogeny of Continents. Macquarie University, Sydney Australia, Macquarie University, Sydney Australia.
Genter, A., Traineau, H., Artignan, D., 1997. Synthesis of Geological and Geophysical Data at Soultz-Sous-Forêts (France) R 39440. BRGM, France.
Genter, A., Homeier, G., Chèvremont, P., Tenzer, H., 1999. Deepening of GPK-2 HDR Borehole, 3880–5090 m (Soultz-Sous-Forêts, France) Geological Monitoring R 40685. BRGM, France.
Genter, A., Guillou-Frottier, L., Feybesse, J.-L., Nicol, N., Dezayes, C., Schwartz, S., 2003. Typology of potential Hot Fractured Rock resources in Europe. Geothermics 32, 701–710. https://doi.org/10.1016/S0375-6505(03)00065-8.
Genter, A., Evans, K., Cuenot, N., Fritsch, D., Sanjuan, B., 2010. Contribution of the exploration of deep crystalline fractured reservoir of Soultz to the knowledge of enhanced geothermal systems (EGS). Compt. Rendus Geosci. 342, 502–516. https://doi.org/10.1016/j.crte.2010.01.006.
Gérard, A., Genter, A., Kohl, T., Lutz, P., Rose, P., Rummel, F., 2006. The deep EGS (Enhanced Geothermal System) project at Soultz-sous-Forêts (Alsace, France). Geothermics 35, 473–483. https://doi.org/10.1016/j.geothermics.2006.12.001.
Geyer, O.F., Gwinner, M.P., Simon, T., 2011. Geologie von Baden-Württemberg, 5th ed. Schweizerbart, Stuttgart. (627 pp.).
Giebel, R.J., Parsapoor, A., Walter, B.F., Braunger, S., Marks, M.A.W., Wenzel, T., Markl, G., 2019. Evidence for magma–wall rock interaction in carbonatites from the Kaiserstuhl Volcanic Complex (Southwest Germany). J. Petrol. 60, 1163–1194. https://doi.org/10.1093/petrology/egz028.
Glaas, C., Vidal, J., Patrier, P., Girard, J.-F., Beaufort, D., Petit, S., Genter, A., 2019. How do secondary minerals in granite help distinguish paleo- from present-day permeable fracture zones? Joint interpretation of SWIR spectroscopy and geophysical logs in the geothermal wells of northern Alsace. Geofluids 2019, 1–20. https://doi.org/10.1155/2019/8231816.
Göb, S., Loges, A., Nolde, N., Bau, M., Jacob, D.E., Markl, G., 2013. Major and trace element compositions (including REE) of mineral, thermal, mine and surface waters in SW Germany and implications for water–rock interaction. Appl. Geochem. 33, 127–152. https://doi.org/10.1016/j.apgeochem.2013.02.006.
Grant, J.A., 1986. The isocon diagram; a simple solution to Gresens' equation for metasomatic alteration. Econ. Geol. 81, 1976–1982. https://doi.org/10.2113/gsecongeo.81.8.1976.
Grant, J.A., 2005. Isocon analysis: a brief review of the method and applications. Phys. Chem. Earth Parts A/B/C 30, 997–1004. https://doi.org/10.1016/j.pce.2004.11.003.
Hann, H.P., Chen, F., Zedler, H., Frisch, W., Loeschke, J., 2003. The Rand Granite in the southern Schwarzwald and its geodynamic significance in the Variscan belt of SW Germany. Geol. Rundsch. 92, 821–842. https://doi.org/10.1007/s00531-003-0361-8.
He, K., Stober, I., Bucher, K., 1999. Chemical evolution of thermal waters from limestone aquifers of the Southern Upper Rhine Valley. Appl. Geochem. 14, 223–235. https://doi.org/10.1016/S0883-2927(98)00046-8.
Held, S., Genter, A., Kohl, T., Kölbel, T., Sausse, J., Schoenball, M., 2014. Economic evaluation of geothermal reservoir performance through modeling the complexity of the operating EGS in Soultz-sous-Forêts. Geothermics 51, 270–280. https://doi.org/10.1016/j.geothermics.2014.01.016.
Hooijkaas, G.R., Genter, A., Dezayes, C., 2006. Deep-seated geology of the granite intrusions at the Soultz EGS site based on data from 5km-deep boreholes. Geothermics 35, 484–506. https://doi.org/10.1016/j.geothermics.2006.03.003.
Jochum, K.P., Nohl, U., Herwig, K., Lammel, E., Stoll, B., Hofmann, A.W., 2005. GeoReM: a new geochemical database for reference materials and isotopic standards. Geostand. Geoanal. Res. 29, 333–338. https://doi.org/10.1111/j.1751-908X.2005.tb00904.x.
Jolie, E., Scott, S., Faulds, J., Chambefort, I., Axelsson, G., Gutiérrez-Negrín, L.C., Regenspurg, S., Ziegler, M., Ayling, B., Richter, A., Zemedkun, M.T., 2021. Geological controls on geothermal resources for power generation. Nat. Rev. Earth Environ. 2, 324–339. https://doi.org/10.1038/s43017-021-00154-y.
Kölbel, L., Kölbel, T., Herrmann, L., Kaymakci, E., Ghergut, I., Poirel, A., Schneider, J., 2023. Lithium extraction from geothermal brines in the Upper Rhine Graben: a case study of potential and current state of the art. Hydrometallurgy 221, 106131. https://doi.org/10.1016/j.hydromet.2023.106131.
Lardeaux, J.M., Schulmann, K., Faure, M., Janoušek, V., Lexa, O., Skrzypek, E., Edel, J.B., Štípská, P., 2014. The Moldanubian Zone in the French Massif Central, Vosges/Schwarzwald and Bohemian Massif revisited: differences and similarities. Geol. Soc. Lond. Spec. Publ. 405, 7–44. https://doi.org/10.1144/SP405.14.
Ledésert, B.A., Hébert, R.L., 2020. How can deep geothermal projects provide information on the temperature distribution in the Upper Rhine Graben? The example of the Soultz-Sous-Forêts-enhanced Geothermal System. Geosciences 10, 459. https://doi.org/10.3390/geo- sciences10110459.
Ledésert, B., Dubois, J., Genter, A., Meunier, A., 1993. Fractal analysis of fractures applied to Soultz-sous-Forets hot dry rock geothermal program. J. Volcanol. Geotherm. Res. 57, 1–17. https://doi.org/10.1016/0377-0273(93)90028-P.
Ledésert, B., Joffre, J., Amblès, A., Sardini, P., Genter, A., Meunier, A., 1996. Organic matter in the Soultz HDR granitic thermal exchanger (France): natural tracer of fluid circulations between the basement and its sedimentary cover. J. Volcanol. Geotherm. Res. 70, 235–253. https://doi.org/10.1016/0377-0273(95)00058-5.
Ledésert, B., Berger, G., Meunier, A., Genter, A., Bouchet, A., 1999. Diagenetic-type reactions related to hydrothermal alteration in the Soultz-sous-Forêts granite, France. Eur. J. Mineral. 11, 731–742. https://doi.org/10.1127/ejm/11/4/0731.
Ledésert, B.A., Hébert, R.L., Genter, A., Bartier, D., Clauer, N., Grall, C., 2010. Fractures, hydrothermal alterations and permeability in the Soultz Enhanced Geothermal System. Compt. Rendus Geosci. 342, 607–615. https://doi.org/10.1016/j.crte.2009.09.011.
LGB-RLP, 2013. Landesamt für Geologie und Bergbau/Kartenviewer. https://mapclient.lgb-rlp.de/?app=lgb&view_id=21. (Accessed 2 March 2023).
LGRB-Kartenviewer, 2021. LGRB-Kartenviewer. Regierungspräsidium Freiburg, Landesamt für Geologie, Rohstoffe und Bergbau. https://maps.lgrb-bw.de/. (Accessed 2 March 2023).
Li, W., Liu, X.-M., 2020. Experimental investigation of lithium isotope fractionation during kaolinite adsorption: implications for chemical weathering. Geochim. Cosmochim. Acta 284, 156–172. https://doi.org/10.1016/j.gca.2020.06.025.
Lippolt, H.J., Schleicher, H., Raczek, I., 1983. Rb-Sr systematics of Permian volcanites in the Schwarzwald (SW-Germany). Contrib. Mineral. Petrol. 84, 272–280. https://doi.org/10.1007/BF00371291.
Loges, A., Wagner, T., Kirnbauer, T., Göb, S., Bau, M., Berner, Z., Markl, G., 2012. Source and origin of active and fossil thermal spring systems, northern Upper Rhine Graben, Germany. Appl. Geochem. 27, 1153–1169. https://doi.org/10.1016/j.apgeochem.2012.02.024.
Lützner, H., Kowalczyk, G., Schneider, J.W., 2012. Stratigraphische Korrelation der innervariscischen Rotliegendbecken in Deutschland. In: Schriftenreihe der Deutschen Gesellschaft für Geowissenschaften, vol. 61, pp. 861–879. https://doi.org/10.1127/sdgg/61/2012/861.
Macpherson, G.L., 2015. Lithium in fluids from Paleozoic-aged reservoirs, Appalachian Plateau region, USA. Appl. Geochem. 60, 72–77. https://doi.org/10.1016/j.apgeochem.2015.04.013.
Marks, M.A., Marschall, H.R., Schühle, P., Guth, A., Wenzel, T., Jacob, D.E., Barth, M., Markl, G., 2013. Trace element systematics of tourmaline in pegmatitic and hydrothermal systems from the Variscan Schwarzwald (Germany): the importance of major element composition, sector zoning, and fluid or melt composition. Chem. Geol. 344, 73–90. https://doi.org/10.1016/j.chemgeo.2013.02.025.
Marza, M., Ferguson, G., Thorson, J., Barton, I., Kim, J.-H., Ma, L., McIntosh, J., 2024. Geological controls on lithium production from basinal brines across North America. J. Geochem. Explor. 257, 107383. https://doi.org/10.1016/j.gexplo.2023.107383.
McCuaig, T.C., Hronsky, J., 2014. The mineral system concept: the key to exploration targeting. In: Kelley, K.D. (Ed.), Building Exploration Capability for the 21st Century. Society of Economic Geologists, Littleton CO. https://doi.org/10.5382/SP.18.08.
McCuaig, T.C., Beresford, S., Hronsky, J., 2010. Translating the mineral systems approach into an effective exploration targeting system. Ore Geol. Rev. 38, 128–138. https://doi.org/10.1016/j.oregeorev.2010.05.008.
MEET project, 2022. Multidisciplinary and multi-context demonstration of EGS exploration and Exploitation Techniques and potentials (MEET). https://www.meet-h2020.com/;. https://cordis.europa.eu/project/id/792037. (Accessed 28 February 2023).
Meyer, M., Brockamp, O., Clauer, N., Renk, A., Zuther, M., 2000. Further evidence for a Jurassic mineralizing event in central Europe: K-Ar dating of hydrothermal alteration and fluid inclusion systematics in wall rocks of the Käfersteige fluorite vein deposit in the northern Black Forest, Germany. Mineral. Deposita 35, 754–761. https://doi.org/10.1007/s001260050277.
Moeck, I.S., 2014. Catalog of geothermal play types based on geologic controls. Renew. Sust. Energ. Rev. 37, 867–882. https://doi.org/10.1016/j.rser.2014.05.032.
Munk, L.A., Hynek, S.A., Bradley, D.C., Boutt, D.F., Labay, K.A., Jochens, H., 2016. Lithium Brines: A Global Perspective. https://doi.org/10.5382/Rev.18.14 (339 pp.).
Nitsch, E., Zedler, H., 2009. Oberkarbon und Perm in Baden-Württemberg. In: Regierungspräsidium Freiburg - Abteilung 9 Landesamt für Geologie, Rohstoffe und Bergbau (Ed.), LGRB-Informationen: Beiträge zur Lithostratigraphie in Baden-Württemberg, vol. 22.
Pauwels, H., Fouillac, C., Fouillac, A.-M., 1993. Chemistry and isotopes of deep geothermal saline fluids in the Upper Rhine Graben: origin of compounds and water-rock inter- actions. Geochim. Cosmochim. Acta 57, 2737–2749. https://doi.org/10.1016/0016-7037(93)90387-C.
Pearce, N.J., Perkins, W.T., Westgate, J.A., Gorton, M.P., Jackson, S.E., Neal, C.R., Chenery, S.P., 1997. A compilation of new and published major and trace element data for NIST SRM 610 and NIST SRM 612 glass reference materials. Geostand. Geoanal. Res. 21, 115–144. https://doi.org/10.1111/j.1751-908X.1997.tb00538.x.
Pfaff, K., Hildebrandt, L.H., Leach, D.L., Jacob, D.E., Markl, G., 2010. Formation of the Wiesloch Mississippi Valley-type Zn-Pb-Ag deposit in the extensional setting of the Upper Rhinegraben, SW Germany. Mineral. Deposita 45, 647–666. https://doi.org/10.1007/s00126-010-0296-5.

Phan, T.T., Capo, R.C., Stewart, B.W., Macpherson, G.L., Rowan, E.L., Hammack, R.W., 2016. Factors controlling Li concentration and isotopic composition in formation waters and host rocks of Marcellus Shale, Appalachian Basin. Chem. Geol. 420, 162–179. https://doi.org/10.1016/j.chemgeo.2015.11.003.

Reich, R., Slunitschek, K., Danisi, R.M., Eiche, E., Kolb, J., 2022. Lithium extraction techniques and the application potential of different sorbents for lithium recovery from brines. Miner. Process. Extr. Metall. Rev. 1–20. https://doi.org/10.1080/08827508.2022.2047041.

Rupf, I., Nitsch, E., 2008. Das Geologische Landesmodell von Baden-Württemberg: Datengrundlagen, technische Umsetzung und erste geologische Ergebnisse. LGRB-Informationen 21, Freiburg i. Br.

Sanjuan, B., Millot, R., Dezayes, C., Brach, M., 2010. Main characteristics of the deep geothermal brine (5km) at Soultz-sous-Forêts (France) determined using geochemical and tracer test data. Compt. Rendus Geosci. 342, 546–559. https://doi.org/10.1016/j.crte.2009.10.009.

Sanjuan, B., Millot, R., Innocent, C., Dezayes, C., Scheiber, J., Brach, M., 2016. Major geochemical characteristics of geothermal brines from the Upper Rhine Graben granitic basement with constraints on temperature and circulation. Chem. Geol. 428, 27–47. https://doi.org/10.1016/j.chemgeo.2016.02.021.

Sanjuan, B., Gourcerol, B., Millot, R., Rettenmaier, D., Jeandel, E., Rombaut, A., 2022. Lithium-rich geothermal brines in Europe: an up-date about geochemical characteristics and implications for potential Li resources. Geothermics 101, 102385. https://doi.org/10.1016/j.geo- thermics.2022.102385.

Scharrer, M., Reich, R., Fusswinkel, T., Walter, B.F., Markl, G., 2021. Basement aquifer evolution and the formation of unconformity-related hydrothermal vein deposits: LA-ICP-MS analyses of single fluid inclusions in fluorite from SW Germany. Chem. Geol. 575, 120260. https://doi.org/10.1016/j.chemgeo.2021.120260.

Scharrer, M., Epp, T., Walter, B., Pfaff, K., Vennemann, T., Markl, G., 2022. The formation of (Ni-Co-Sb)-Ag-As ore shoots in hydrothermal galena-sphalerite-fluorite veins. Mineral. Deposita 57, 853–885. https://doi.org/10.1007/s00126-021-01059-y.

Schill, E., Genter, A., Cuenot, N., Kohl, T., 2017. Hydraulic performance history at the Soultz EGS reservoirs from stimulation and long-term circulation tests. Geothermics 70, 110–124. https://doi.org/10.1016/j.geothermics.2017.06.003.

Schleicher, A.M., Warr, L.N., Kober, B., Laverret, E., Clauer, N., 2006. Episodic mineralization of hydrothermal illite in the Soultz-sous-Forêts granite (Upper Rhine Graben, France). Contrib. Mineral. Petrol. 152, 349–364. https://doi.org/10.1007/s00410-006-0110-7.

Schmidt, R.B., Bucher, K., Stober, I., 2018. Experiments on granite alteration under geothermal reservoir conditions and the initiation of fracture evolution. Eur. J. Mineral. 30, 899–916. https://doi.org/10.1127/ejm/2018/0030-2771.

Schroth, B.K., Sposito, G., 1997. Surface charge properties of kaolinite. Clay Clay Miner. 45, 85–91. https://doi.org/10.1346/CCMN.1997.0450110.

Skrzypek, E., Schulmann, K., Tabaud, A.-S., Edel, J.-B., 2014. Palaeozoic evolution of the Variscan Vosges Mountains. Geol. Soc. Lond. Spec. Publ. 405, 45–75. https://doi.org/10.1144/sp405.8.

Staude, S., Bons, P.D., Markl, G., 2009. Hydrothermal vein formation by extension-driven dewatering of the middle crust: an example from SW Germany. Earth Planet. Sci. Lett. 286, 387–395. https://doi.org/10.1016/j.epsl.2009.07.012.

Steiger, K., Reich, R., Slunitschek, K., Steinmüller, K., Bergemann, C., Hilgers, C., Kolb, J., 2022. Lithium in Europa. THINKTANK für Industrielle Ressourcenstrategien, Karlsruhe. https://doi.org/10.5445/IR/1000154047.

Stober, I., Bucher, K., 1999a. Deep groundwater in the crystalline basement of the Black Forest region. Appl. Geochem. 14, 237–254. https://doi.org/10.1016/S0883-2927(98)00045-6.

Stober, I., Bucher, K., 1999b. Origin of salinity of deep groundwater in crystalline rocks. Terra Nova 11, 181–185. https://doi.org/10.1046/j.1365-3121.1999.00241.x.

Stober, I., Bucher, K., 2007. Hydraulic properties of the crystalline basement. Hydrogeol. J. 15, 213–224. https://doi.org/10.1007/s10040-006-0094-4.

Stober, I., Bucher, K., 2015a. Hydraulic and hydrochemical properties of deep sedimentary reservoirs of the Upper Rhine Graben, Europe. Geofluids 15, 464–482. https://doi.org/10.1111/gfl.12122.

Stober, I., Bucher, K., 2015b. Hydraulic conductivity of fractured upper crust: insights from hydraulic tests in boreholes and fluid-rock interaction in crystalline basement rocks. Geofluids 15, 161–178. https://doi.org/10.1111/gfl.12104.

Stussi, J.-M., Cheilletz, A., Royer, J.-J., Chèvremont, P., Féraud, G., 2002. The Hidden Monzogranite of Soultz-Sous-Forêts (Rhine Graben, France): Mineralogy, Petrology and Genesis. Géologie de la France, pp. 45–64.

Tabaud, A.-S., Whitechurch, H., Rossi, P., Schulmann, K., Guerrot, C., Cocherie, A., 2014. Devonian–Permian magmatic pulses in the northern Vosges Mountains (NE France): result of continuous subduction of the Rhenohercynian Ocean and Avalonian passive margin. Geol. Soc. Lond. Spec. Publ. 405, 197–223. https://doi.org/10.1144/SP405.12.

Tabaud, A.-S., Janoušek, V., Skrzypek, E., Schulmann, K., Rossi, P., Whitechurch, H., Guerrot, C., Paquette, J.-L., 2015. Chronology, petrogenesis and heat sources for successive Carboniferous magmatic events in the Southern–Central Variscan Vosges Mts (NE France). J. Geol. Soc. Lond. 172, 87–102. https://doi.org/10.1144/jgs2013-123.

Timar-Geng, Z., Fügenschuh, B., Wetzel, A., Dresmann, H., 2006. Low-temperature thermochronology of the flanks of the southern Upper Rhine Graben. Int. J. Earth Sci. 95, 685–702. https://doi.org/10.1007/s00531-005-0059-1.

Tischendorf, G., Rieder, M., Förster, H.-J., Gottesmann, B., Guidotti, C.V., 2004. A new graphical presentation and subdivision of potassium micas. Mineral. Mag. 68, 649–667. https://doi.org/10.1180/0026461046840210.

UnLimited project, 2022. UnLimited, Hydrosion GmbH. https://geothermal-lithium.org/.

Vaida, M., Hann, H.P., Sawatzki, G., Frisch, W., 2004. Ordovician and Silurian protolith ages of metamorphosed clastic sedimentary rocks from the southern Schwarzwald, SW Germany: a palynological study and its bearing on the Early Palaeozoic geotectonic evolution. Geol. Mag. 141, 629–643. https://doi.org/10.1017/S0016756804009641.

Vidal, J., Genter, A., 2018. Overview of naturally permeable fractured reservoirs in the central and southern Upper Rhine Graben: insights from geothermal wells. Geothermics 74, 57–73. https://doi.org/10.1016/j.geothermics.2018.02.003.

Vidal, J., Patrier, P., Genter, A., Beaufort, D., Dezayes, C., Glaas, C., Lerouge, C., Sanjuan, B., 2018. Clay minerals related to the circulation of geothermal fluids in boreholes at Rittershoffen (Alsace, France). J. Volcanol. Geotherm. Res. 349, 192–204. https://doi.org/10.1016/j.jvolgeores.2017.10.019.

Voges, A., Toloczyki, M., Zitzmann, A., Wittekindt, H., Trurnit, P., 2006. Geologische Karte der Bundesrepublik Deutschland 1:1.000.000 (GK1000). Geological Map of Germany 1:1,000,000 (GK1000), 4th ed. Bundesanstalt für Geowissenschaften und Rohstoffe (BGR), Hannover, Germany.

Vulcan Energie Ressourcen GmbH, 2023. Vulcan Zero Carbon Lithium™ project phase one DFS results and resources-reserves update, Karlsruhe. https://www.investi.com.au/api/announcements/vul/e617fca6-6d4.pdf. (Accessed 28 February 2023).

Walter, B.F., Immenhauser, A., Geske, A., Markl, G., 2015. Exploration of hydrothermal carbonate magnesium isotope signatures as tracers for continental fluid aquifers, Schwarzwald mining district, SW Germany. Chem. Geol. 400, 87–105. https://doi.org/10.1016/j.chemgeo.2015.02.009.

Walter, B.F., Burisch, M., Markl, G., 2016. Long-term chemical evolution and modification of continental basement brines - a field study from the Schwarzwald, SW Germany. Geofluids 16, 604–623. https://doi.org/10.1111/gfl.12167.

Walter, B.F., Burisch, M., Marks, M.A.W., Markl, G., 2017. Major element compositions of fluid inclusions from hydrothermal vein-type deposits record eroded sedimentary units in the Schwarzwald district, SW Germany. Mineral. Deposita 52, 1191–1204. https://doi.org/10.1007/s00126-017-0719-7.

Walter, B.F., Burisch, M., Fusswinkel, T., Marks, M.A.W., Steele-MacInnis, M., Wälle, M., Apukhtina, O.B., Markl, G., 2018a. Multi-reservoir fluid mixing processes in rift-related hydrothermal veins, Schwarzwald, SW-Germany. J. Geochem. Explor. 186, 158–186. https://doi.org/10.1016/j.gexplo.2017.12.004.

Walter, B.F., Gerdes, A., Kleinhanns, I.C., Dunkl, I., von Eynatten, H., Kreissl, S., Markl, G., 2018b. The connection between hydrothermal fluids, mineralization, tectonics and magmatism in a continental rift setting: fluorite Sm-Nd and hematite and carbonates U-Pb geochronology from the Rhinegraben in SW Germany. Geochim. Cosmochim. Acta 240, 11–42. https://doi.org/10.1016/j.gca.2018.08.012.

Walter, B.F., Kortenbruck, P., Scharrer, M., Zeitvogel, C., Wälle, M., Mertz-Kraus, R., Markl, G., 2019. Chemical evolution of ore-forming brines – basement leaching, metal provenance, and the redox link between barren and ore-bearing hydrothermal veins. A case study from the Schwarzwald mining district in SW-Germany. Chem. Geol. 506, 126–148. https://doi.org/10.1016/j.chemgeo.2018.12.038.

Walter, B.F., Jensen, J.L., Coutinho, P., Laurent, O., Markl, G., Steele-MacInnis, M., 2020a. Formation of hydrothermal fluorite-hematite veins by mixing of continental basement brine and redbed-derived fluid: Schwarzwald mining district, SW-Germany. J. Geochem. Explor. 212, 106512. https://doi.org/10.1016/j.gexplo.2020.106512.

Walter, B.F., Scharrer, M., Burisch, M., Apukhtina, O.B., Markl, G., 2020b. Limited availability of sulfur promotes copper-rich mineralization in hydrothermal Pb-Zn veins: a case study from the Schwarzwald, SW Germany. Chem. Geol. 532, 119358. https://doi.org/10.1016/j. chemgeo.2019.119358.

Warr, L.N., 2020. Recommended abbreviations for the names of clay minerals and associated phases. Clay Miner. 55, 261–264. https://doi.org/10.1180/clm.2020.30.

Warr, L.N., 2021. IMA-CNMNC approved mineral symbols. Mineral. Mag. 85, 291–320. https://doi.org/10.1180/mgm.2021.43.

Weldeghebriel, M.F., Lowenstein, T.K., 2023. Seafloor hydrothermal systems control long-term changes in seawater Li+: evidence from fluid inclusions. Sci. Adv. 9, eadf1605. https://doi.org/10.1126/sciadv.adf1605.

Yuan, G., Cao, Y., Schulz, H.-M., Hao, F., Gluyas, J., Liu, K., Yang, T., Wang, Y., Xi, K., Li, F., 2019. A review of feldspar alteration and its geological significance in sedimentary basins: from shallow aquifers to deep hydrocarbon reservoirs. Earth Sci. Rev. 191, 114–140. https://doi.org/10.1016/j.earscirev.2019.02.004.

Ziegler, P.A., 1992. European Cenozoic rift system. Tectonophysics 208, 91–111. https://doi.org/10.1016/0040-1951(92)90338-7.

Ziegler, P.A., Dèzes, P., 2005. Evolution of the lithosphere in the area of the Rhine Rift System. Int. J. Earth Sci. 94, 594–614. https://doi.org/10.1007/s00531-005-0474-3.

Ziegler, P.A., Schumacher, M.E., Dèzes, P., van Wees, J.-D., Cloetingh, S., 2004. Post-Variscan evolution of the lithosphere in the Rhine Graben area: constraints from subsidence modeling. Geol. Soc. Lond. Spec. Publ. 223, 289–317. https://doi.org/10.1144/GSL.SP.2004.223.01.13.